Prepared for submission to JCAP

On the regularity of the covariance matrix of a discretized scalar field on the sphere

J. D. Bilbao-Ahedo[a,b] **R. B. Barreiro**[b] **D. Herranz**[b] **P. Vielva**[b] **E. Martínez-González**[b]

[a]Departamento de Física Moderna, Universidad de Cantabria,
Av. los Castros s/n, 39005 Santander (Spain)
[b]Instituto de Física de Cantabria (CSIC-UC),
Av. los Castros s/n, 39005 Santander (Spain)

E-mail: bilbao@ifca.unican.es, barreiro@ifca.unican.es, herranz@ifca.unican.es, vielva@ifca.unican.es, martinez@ifca.unican.es

Abstract. We present a comprehensive study of the regularity of the covariance matrix of a discretized field on the sphere. In a particular situation, the rank of the matrix depends on the number of pixels, the number of spherical harmonics, the symmetries of the pixelization scheme and the presence of a mask. Taking into account the above mentioned components, we provide analytical expressions that constrain the rank of the matrix. They are obtained by expanding the determinant of the covariance matrix as a sum of determinants of matrices made up of spherical harmonics. We investigate these constraints for five different pixelizations that have been used in the context of Cosmic Microwave Background (CMB) data analysis: `Cube`, `Icosahedron`, `Igloo`, `GLESP` and `HEALPix`, finding that, at least in the considered cases, the `HEALPix` pixelization tends to provide a covariance matrix with a rank closer to the maximum expected theoretical value than the other pixelizations. The effect of the propagation of numerical errors in the regularity of the covariance matrix is also studied for different computational precisions, as well as the effect of adding a certain level of noise in order to regularize the matrix. In addition, we investigate the application of the previous results to a particular example that requires the inversion of the covariance matrix: the estimation of the CMB temperature power spectrum through the Quadratic Maximum Likelihood algorithm. Finally, some general considerations in order to achieve a regular covariance matrix are also presented.

Keywords: CMBR theory, CMBR experiments.

arXiv:1701.06617v1 [astro-ph.CO] 23 Jan 2017

Contents

1 Introduction **1**

2 The rank of the covariance matrix **3**

3 The effect of symmetries on the rank of C **5**
3.1 S_I symmetry: $\mathbf{r} \to -\mathbf{r}$ 5
3.2 S_{II} symmetry: $\phi \to \phi + \pi$ 6
3.3 S_{III} symmetry: $\phi \to \phi + \pi/2$ 7

4 Results for different pixelization schemes **7**
4.1 `Cube` 9
4.2 `Icosahedron` 11
4.3 `Igloo` 12
4.4 `GLESP` 13
4.5 `HEALPix` 14

5 Effect of the power spectrum and the beam transfer function **16**

6 Effect of noise **17**

7 Effect of masking **19**

8 Application to the QML method **20**

9 Conclusions **25**

A Study of the determinant of C **27**

B S_I symmetry: $\mathbf{r} \to -\mathbf{r}$ **28**

C S_{II} symmetry: $\phi \to \phi + \pi$ **29**

D S_{III} symmetry: $\phi \to \phi + \pi/2$ **31**

E Rank expression under the presence of a mask **32**

1 Introduction

With the advent of the precision era of Cosmology and 'big data' astrophysical experiments, data analysis techniques have risen to a prominent role in modern Astronomy. In particular, the treatment of very large matrices is a challenge from the point of view of algebraic and numerical methods, data storage and software implementation. For example, many astrophysical problems require the manipulation of large covariance matrices and their inverses. But it is often the case that such matrices are ill-conditioned and their inverse matrices cannot be calculated; when this happens, the problem must be attacked either by means of clever

algorithms that calculate the pseudo-inverse of the matrix [see, e.g., 1] or by *ad hoc* regularizers such as the addition of a small amount of uncorrelated noise to the diagonal of the covariance matrix.

The literature is rich in situations where the regularity of the covariance matrix plays a fundamental role. For example, the inverse of the covariance matrix is necessary for the study of the statistics of the Cosmic Microwave Background (CMB), the Quadratic Maximum Likelihood (QML) power spectrum estimator [2], the maximum likelihood cosmological parameter estimation [4, 5], to study the topology of the universe [6] and for many CMB foreground removal/component separation methods [see, e.g., 7–10]. Beyond the mere characterization of the second-order statistics of the CMB temperature or polarization fluctuations, covariance matrices are also fundamental for the study of non-Gaussianity [11, 12] and the statistical analysis of CMB anomalies such as the Cold Spot [13]. But the covariance matrix is often ill-conditioned even for low resolution sky maps.

The typical solution consists on the regularization 'by hand' of the covariance matrix. For example a small level of white noise is added to the noise covariance matrix of the CMB temperature data involved in the construction of the low-multipole Planck likelihood [5]. Another possibility is to deal with ill-conditioned covariance matrices by using a principal component analysis approach to remove the lowest degenerate eigenvalues, as is done for instance to study the multi-normality of the CMB [14] or in the estimation of primordial non-Gaussianity using wavelets [12]. The main problem with this kind of approaches is the *ad hoc* nature of the regularization. For example, the amount of uncorrelated artificial noise to be added to the covariance matrix must be carefully chosen: if the level of the noise is too small, it may not suffice to make the matrix regular, but if it is too large, the quality of the data is sorely compromised. One must find the correct amount of noise by trial and error.

A more fundamental question is why and how covariance matrices become ill-conditioned. By definition, all covariance matrices should be positive-semidefinite and symmetric. Therefore, a covariance matrix can be singular if it has, at least, one eigenvalue equal to zero. However, in practice it is often assumed that if a covariance matrix arising from CMB data is singular, it must be so because of numerical issues related to the way the inverse is computed and to limits in computer precision. In this paper we will focus on the interesting case of observations on the sphere, and we will make a comprehensive study on how the regularity and rank of the covariance matrix depend on how it is built, the pixelization scheme, the sky coverage and the regularizing noise. We will show that, even with arbitrary high precision, CMB covariance matrices can be singular due to the way the CMB is sampled. As we will see in the following sections, the way the sphere is pixelised can introduce symmetries that affect the regularity of covariance matrices. This is a purely algebraic effect that, as far as we know, has not been explored in the literature before.

The structure of the paper is as follows: section 2 enunciates a general constraint in the rank of the covariance matrix. Section 3 presents further upper limits on the rank under the presence of some specific symmetries of the pixelization. These constraints are tested for five different pixelization schemes in section 4. Section 5 studies the effect of introducing a realistic CMB model when computing the covariance matrix as well as the degrading effect of numerical precision. Section 6 investigates the addition of noise as a regulariser of the covariance matrix. The effect of the presence of a mask in the rank of the covariance matrix is addressed in section 7. As an example, section 8 applies the results of the previous sections to the Quadratic Maximum Likelihood method [2] for the estimation of the angular power spectrum, which requires the calculation of the inverse of the covariance matrix. Concluding

remarks are offered in section 9. Finally, technical points related to the covariance matrix are presented in the appendices.

2 The rank of the covariance matrix

If a discretized scalar field on the sphere arises from isotropic random fluctuations, the elements of the covariance matrix $\mathbf{C} \equiv \langle \mathbf{x}\mathbf{x}^t \rangle$ can be written in terms of the angular power spectrum C_ℓ as:

$$\mathbf{C}_{ij} = \sum_{\ell=0}^{\infty} C_\ell \sum_{m=-\ell}^{\ell} Y_{\ell m}(\theta_i, \phi_i) Y^*_{\ell m}(\theta_j, \phi_j), \tag{2.1}$$

where $Y_{\ell m}$ are the spherical harmonics given by:

$$Y_{\ell m}(\theta, \phi) = \sqrt{\frac{2\ell+1}{4\pi} \frac{(l-m)!}{(l+m)!}} P_{\ell m}(\cos\theta) e^{im\phi}, \tag{2.2}$$

and $P_{\ell m}$ are the associated Legendre polynomials. In real life applications, the sum over multipoles does not extend to infinity, but it has a cutoff at some $\ell_{\rm max}$ instead. If the value of $\ell_{\rm max}$ is not sufficiently large, the covariance matrix can be singular. This is a problem for all numerical applications that require the inversion of $\mathbf{C}$. On the other hand, a too large value of $\ell_{\rm max}$ can lead to extremely heavy computational costs. Besides, there is a limit in the spatial resolution that can be explored, which is determined by the lowest angular distance between points in the pixelization, as established by the Nyquist's theorem. Therefore, one must be very careful with the choice of $\ell_{\rm max}$. In this section we will make a thorough study of the rank of $\mathbf{C}$ as a function of $\ell_{\rm max}$.

Let $\ell_{\rm min}$ and $\ell_{\rm max}$ be the summation limits in the finite version of eq. (2.1). Let us also consider a pixelization of the sky such that the unit sphere is sampled at a set of n positions $\{\mathbf{r}_i\}$ and angular coordinates $\{(\theta_i, \phi_i)\}$, $i = 1, \ldots, n$. In order to simplify the notation in the following expressions, we introduce the univocal index change $(\ell, m) \leftrightarrow \mu$ for the spherical harmonics such that:

$$\mu\,(\ell, m) = \sum_{k=\ell_{\rm min}}^{\ell-1} (2k+1) + \ell + m + 1 = \ell^2 - \ell_{\rm min}^2 + \ell + m + 1. \tag{2.3}$$

This change assigns a unique μ to each pair (ℓ, m) in ascending m order, that is, $\mu(\ell_{\rm min}, -\ell_{\rm min}) = 1$, $\mu(\ell_{\rm min}, -\ell_{\rm min}+1) = 2$ and so on. μ runs from 1 to N, the total number of spherical harmonics, given by:

$$N = \sum_{\ell=\ell_{\rm min}}^{\ell_{\rm max}} (2\ell+1) = \ell_{\rm max}^2 - \ell_{\rm min}^2 + 2\ell_{\rm max} + 1. \tag{2.4}$$

We will also use the same index μ for the power spectrum, such that C_μ corresponds to the power of the multipole ℓ obtained as:

$$\ell = \text{floor}\left(\sqrt{\ell_{\rm min}^2 - 1 + \mu}\right), \tag{2.5}$$

where floor(x) is the largest integer not greater than x. Using this notation, we can write:

$$Y_{\ell m}(\theta_i, \phi_i) = Y_\mu(\theta_i, \phi_i) = Y_{\mu i}, \tag{2.6}$$

and thus:

$$\mathbf{C}_{ij} = \sum_{\ell=\ell_{\min}}^{\ell_{\max}} C_\ell \sum_{m=-\ell}^{\ell} Y_{\ell m}(\theta_i, \phi_i) Y^*_{\ell m}(\theta_j, \phi_j) = \sum_{\mu=1}^{N} C_\mu Y_{\mu i} Y^*_{\mu j}, \tag{2.7}$$

where μ makes reference to the harmonic indexes, and i and j make reference to the pair of points on the sky at which the sum is being calculated. Using this notation, the j^{th} vector column of $\mathbf{C}$ is:

$$\mathbf{C}_{\texttt{Col}_j} = \sum_{\mu_j} C_{\mu_j} \begin{pmatrix} Y_{\mu_j 1} \\ Y_{\mu_j 2} \\ \vdots \\ Y_{\mu_j n} \end{pmatrix} Y^*_{\mu_j j}, \tag{2.8}$$

and therefore $\mathbf{C}$ is:

$$\mathbf{C} = \begin{pmatrix} \sum_{\mu_1} C_{\mu_1} \begin{pmatrix} Y_{\mu_1 1} \\ \vdots \\ Y_{\mu_1 n} \end{pmatrix} Y^*_{\mu_1 1} & \cdots & \sum_{\mu_n} C_{\mu_n} \begin{pmatrix} Y_{\mu_n 1} \\ \vdots \\ Y_{\mu_n n} \end{pmatrix} Y^*_{\mu_n n} \end{pmatrix}. \tag{2.9}$$

Using eq. (2.9) and the properties of matrix determinants, we can write the determinant of $\mathbf{C}$ as:

$$|\mathbf{C}| = \sum_{\mu_1 \cdots \mu_n = 1}^{N} \left(\prod_{i=1}^{n} C_{\mu_i} Y^*_{\mu_i i} \right) \begin{vmatrix} Y_{\mu_1 1} & \cdots & Y_{\mu_n 1} \\ \vdots & & \vdots \\ Y_{\mu_1 n} & \cdots & Y_{\mu_n n} \end{vmatrix}. \tag{2.10}$$

We are interested in knowing whether or not $|\mathbf{C}| = 0$. A sufficient condition for this determinant to be zero is that all the determinants of the previous equation are null.

If we calculate $\mathbf{C}$ on n points on the sphere using N spherical harmonics, the number of elements of the sum given in eq. (2.10) is N^n. Any of those determinants can be different from zero if its columns are linearly independent. Since the necessary condition for this to be achieved is that each column corresponds to a different spherical harmonic, we have a first constraint on $\ell_{\max}$: N must be equal or greater than n. In other words, the number of spherical harmonics must be at least as large as the number of considered pixels on the sphere. The rank of the covariance matrix $\mathbf{C}$ is thus constrained by:

$$\text{rank}(\mathbf{C}) \leq \min\left(n, \ell^2_{\max} - \ell^2_{\min} + 2\ell_{\max} + 1\right). \tag{2.11}$$

Hereinafter we will refer to this constraint as R_0.

According to eq. (2.10), if one determinant in the sum is not null, there will be other $n! - 1$ terms that are not zero as well, which correspond to the permutations of its columns. However, we may wonder if the sum of all these elements could be zero. In appendix A we show that the sum of these terms is a real positive number and, therefore, if there exists at least one non-null determinant, then $|\mathbf{C}| > 0$ is satisfied. Nonetheless, note that having $N \geq n$ does not guarantee that this is fulfilled. In particular, even if all the columns of the determinants correspond to different spherical harmonics, they can still be linearly dependent. A particular case when this can happen is under the presence of certain symmetries in the considered pixelization of the sphere. This is studied in more detail in the next section.

3 The effect of symmetries on the rank of C

It is possible that the rank of $\mathbf{C}$ is reduced if the positions where the covariance matrix is calculated have certain symmetries. In this section we will study several of these symmetries, which appear in some commonly used pixelizations of the sphere, and their effect on the rank of $\mathbf{C}$.

As detailed in section 2, the determinant of $\mathbf{C}$ can be expanded as the sum of the determinants of several matrices according to eq. (2.10). It is easy to see that many of these matrices will have a null determinant but, if the sum runs up to a sufficiently large ℓ, some of them might have non-zero determinants. Rather than inspecting the rank of each individual matrix, it is possible to determine the existence (or non existence) of full-rank matrices in eq. (2.10) by inspecting the (non necessarily square) matrix, whose elements are given by:

$$\mathbf{Y} = \begin{pmatrix} Y_{1,1} & \cdots & Y_{N,1} \\ \vdots & & \vdots \\ Y_{1,n} & \cdots & Y_{N,n} \end{pmatrix}, \tag{3.1}$$

where the harmonics are calculated for all the n pixels and N is the number of spherical harmonics. Therefore, $\mathbf{Y}$ is an $n \times N$ matrix, with as many rows as pixels and as many columns as spherical harmonics. For convenience, the value of the element ij of $\mathbf{Y}$ is the value of the spherical harmonic of index $\mu = j$ on the pixel $\mathbf{r}_i$, $\mathbf{Y}_{ij} = Y_{ji} = Y_j(\mathbf{r}_i)$.

It is easy to see that $\mathrm{rank}(\mathbf{C}) = \mathrm{rank}(\mathbf{Y})$. In particular, if $N \geq n$, the maximum possible rank of $\mathbf{Y}$ will be n. If this rank is achieved, this implies that there exists at least n linearly independent columns in $\mathbf{Y}$ and, thus, there is at least one determinant in eq. (2.10) together with its permutations which are different from zero.

With the help of the matrix $\mathbf{Y}$ and defining a diagonal signal matrix $\mathbf{S}$, $\mathbf{S}_{\mu\nu} = C_\mu \delta_{\mu\nu}$, we can get to the same conclusion by a different route. The expression (2.7) can be written as a product of matrices, $\mathbf{C} = \mathbf{Y}\mathbf{S}\mathbf{Y}^\dagger$. Since the rank of the product of matrices is lower than or equal to the minimum rank of the factors, for $\mathbf{C}$ to be regular the number of columns of $\mathbf{Y}$ (the number of spherical harmonics) has to be equal to or greater than the dimensions of $\mathbf{C}$ (the number of pixels).[1]

In the next subsections we will study how the rank of $\mathbf{Y}$ is affected by some specific symmetries.

3.1 S_I symmetry: $\mathbf{r} \to -\mathbf{r}$

First of all, we will consider a pixelization such that all points in the sphere have a diametrically opposed point. For full sky coverage, one would expect that this condition is in general fulfilled since it is reasonable that two symmetrical hemispheres are pixelised in the same way. However, this may not be the case when only partial coverage of the sky is considered.

Let us make the variable change $\cos\theta = z$ in $Y_{\ell m}(\theta, \phi)$. The spherical harmonics $Y_{\ell m}(z, \phi)$ have a well-defined parity with respect to the change $(z, \phi) \to (-z, \phi + \pi)$ (i.e. $\mathbf{r} \to -\mathbf{r}$):

$$Y_{\ell m}(-z, \phi + \pi) = (-1)^\ell Y_{\ell m}(z, \phi). \tag{3.2}$$

[1] This approach can be useful to analyse the rank of the polarization covariance matrix. In this case, the matrix $\mathbf{Y}$ is composed of spherical harmonics of spin 0 and combinations of harmonics of spin ± 2 [3]. The number of rows of $\mathbf{Y}$ is $3 \times n$ and the number of columns is $3 \times N$. Therefore, $\ell_{\max}$ has to be so that $N \geq n$.

Assuming that we have a pixelization and sky coverage such that for each pixel with direction $\mathbf{r}$ there exists a pixel in the direction $-\mathbf{r}$, eq. (3.2) allows us to transform the matrix of eq. (3.1) into a block-diagonal matrix with the same rank as the matrix $\mathbf{Y}$:

$$\mathbf{Y} \to \begin{pmatrix} \mathbf{Y}_e & \mathbf{0} \\ \mathbf{0} & \mathbf{Y}_o \end{pmatrix}, \tag{3.3}$$

where $\mathbf{Y}_e$ is a block of spherical harmonics of even ℓ calculated on half of the points of the pixelization, and $\mathbf{Y}_o$ contains the spherical harmonics with odd ℓ (see appendix B for details).

Therefore, we can write $\text{rank}(\mathbf{Y}) = \text{rank}(\mathbf{Y}_e) + \text{rank}(\mathbf{Y}_o)$. Since the rank of each block is limited by the minimum value of the number of rows and the number of columns, the following constraint must be satisfied:

$$\text{rank}(\mathbf{Y}) \leq \min(N_e, n/2) + \min(N_o, n/2), \tag{3.4}$$

where

$$N_e = \sum_{\substack{\ell=\ell_{\min} \\ (\ell \text{ even})}}^{\ell_{\max}} (2\ell+1), \qquad N_o = \sum_{\substack{\ell=\ell_{\min} \\ (\ell \text{ odd})}}^{\ell_{\max}} (2\ell+1). \tag{3.5}$$

Hereinafter we will refer to the relationship (3.4) as R_1. As will be shown below, this additional constraint can lead in certain cases to the reduction of the maximum rank that the covariance matrix can achieve. In particular, this could yield to a singular covariance matrix even in the case $N \geq n$.

3.2 S_{II} symmetry: $\phi \to \phi + \pi$

Let us assume that we have a pixelization that, in addition to the previous symmetry S_I, satisfies that for each point with coordinates (z, ϕ) there is a point with coordinates $(z, \phi+\pi)$.

Taking into account the following expression of the spherical harmonics:

$$Y_{\ell m}(z, \phi + \pi) = (-1)^m Y_{\ell m}(z, \phi), \tag{3.6}$$

we can further expand the matrix $\mathbf{Y}$ in blocks (see appendix C for details):

$$\mathbf{Y} \to \begin{pmatrix} \mathbf{Y}_{eo} & \mathbf{0} & & \\ \mathbf{0} & \mathbf{Y}_{ee} & \mathbf{0} & \\ & & \mathbf{Y}_{oo} & \mathbf{0} \\ & \mathbf{0} & \mathbf{0} & \mathbf{Y}_{oe} \end{pmatrix}, \tag{3.7}$$

where, for example, $\mathbf{Y}_{eo}$ denotes the block made up of the spherical harmonics of even ℓ and odd m. The size of the blocks depends on the number of pixels at $z = 0$ in the pixelization. The reason is that the pair of points at $z = 0$ that satisfy the symmetry S_{II} also satisfy S_I, so they have to be accounted for in a slightly different way. In particular, appendix C shows that if the map contains u pixels at $z = 0$ and $0 \leq \phi < \pi$, and k pixels at $z > 0$ (note that $k + u = n/2$), then the blocks $\mathbf{Y}_{eo}$ and $\mathbf{Y}_{oe}$ have $k/2$ rows each, and the blocks $\mathbf{Y}_{ee}$ and $\mathbf{Y}_{oo}$ have $k/2+u$ rows each (note that if $u = 0$, the number of rows of each block defaults to $n/4$). Therefore, the rank of the matrix will be limited by the following expression (R_2):

$$\begin{aligned} \text{rank}(\mathbf{Y}) \leq\ & \min(N_{eo}, k/2) + \min(N_{ee}, k/2 + u) \\ & + \min(N_{oo}, k/2 + u) + \min(N_{oe}, k/2), \end{aligned} \tag{3.8}$$

where N_{eo} is the number of spherical harmonics of even ℓ and odd m, N_{ee} is the number of spherical harmonics of even ℓ and even m, and so on.

3.3 S_{III} symmetry: $\phi \to \phi + \pi/2$

Let us assume that we have a pixelization that satisfies the symmetry S_I and that for each pixel at (θ, ϕ) there is a corresponding pixel at $(\theta, \phi+\pi/2)$. Note that, under these conditions, S_{II} is also fulfilled. Under the transformation $\phi \to \phi + \pi/2$ we have:

$$Y_{\ell m}(\theta, \phi + \pi/2) = i^m Y_{\ell m}(\theta, \phi), \tag{3.9}$$

which can be used to transform each non-null block in eq. (3.7) into a new block-diagonal structure (see appendix D). For example, the block $\mathbf{Y}_{eo}$ can be transformed:

$$\mathbf{Y}_{eo} \to \begin{pmatrix} \mathbf{Y}_{e1} & \mathbf{0} \\ \mathbf{0} & \mathbf{Y}_{e3} \end{pmatrix}. \tag{3.10}$$

At the end of this process we have decomposed matrix $\mathbf{Y}$ into a matrix with eight blocks in the diagonal:

$$\{\mathbf{Y}_{e1}, \mathbf{Y}_{e3}, \mathbf{Y}_{e0}, \mathbf{Y}_{e2}, \mathbf{Y}_{o1}, \mathbf{Y}_{o3}, \mathbf{Y}_{o0}, \mathbf{Y}_{o2}\}. \tag{3.11}$$

The corresponding rank is limited by the expression (R_3):

$$\begin{aligned} \mathrm{rank}(\mathbf{Y}) \leq\ & \min(N_{e1}, k/4) + \min(N_{e3}, k/4) \\ & + \min(N_{e0}, k/4 + u/2) + \min(N_{e2}, k/4 + u/2) \\ & + \min(N_{o1}, k/4 + u/2) + \min(N_{o3}, k/4 + u/2) \\ & + \min(N_{o0}, k/4) + \min(N_{o2}, k/4), \end{aligned} \tag{3.12}$$

where k and u have the same meaning as in section 3.2. N_{eq} is the number of spherical harmonics of even ℓ and $q = \mathrm{mod}(m, 4)$.[2] N_{oq} is the number of spherical harmonics of odd ℓ and $q = \mathrm{mod}(m, 4)$. Note that he sum of the eight N_{pq} adds up the total number of spherical harmonics:

$$\sum_{q=0}^{3} N_{eq} + \sum_{q=0}^{3} N_{oq} = \sum_{\ell=2}^{\ell_{\max}} 2\ell + 1. \tag{3.13}$$

Similarly, the sum of the pixels involved in the eight terms of eq. (3.12) adds up to $2k + 2u$, i.e. the total number of pixels n.

4 Results for different pixelization schemes

The particular way in which the sphere is pixelised gives rise to different symmetries and sets of pairs (θ, ϕ), and therefore will have an impact on the rank of the covariance matrix. In this section we will compare the theoretical ranks imposed by the constraints introduced in the previous sections with those obtained for different pixelization schemes. In particular, we will consider five different pixelizations that have been used used to analyse CMB data: `Cube` [15], `Icosahedron` [16], `Igloo` [17], `GLESP` [18] and `HEALPix` [19].

However, before considering these particular pixelization schemes, let us study the case of a generic pixelization that successively fulfils symmetries S_I, S_{II} and S_{III}. We can easily calculate the maximum rank for the covariance matrix for a certain maximum multipole

[2] $\mathrm{mod}(i, j) = i - j \times \mathrm{floor}(i/j)$ denotes the modulo of i and j. In our case, $q = \mathrm{mod}(m, 4)$ can take four different values corresponding to $\{0, 1, 2, 3\}$. Note that for positive m, this quantity is simply given by the rest of m divided by 4.

$N_{\rm pix}$	12			48			192			768		
$\ell_{\rm max}$	2	3	4	5	6	7	12	13	14	26	27	28
Cons.												
R_0	5	12	12	32	45	48	165	192	192	725	768	768
R_1	5	11	12	32	42	48	165	186	192	725	761	768
R_2	5	11	12	32	42	48	165	186	192	725	761	768
R_3	5	11	12	32	42	48	165	186	192	725	761	768

$N_{\rm pix}$	3072					12288			49152		
$\ell_{\rm max}$	53	54	55	56	109	110	111	220	221	222	
Cons.											
R_0	2912	3021	3072	3072	12096	12288	12288	48837	49152	49152	
R_1	2912	3018	3072	3072	12096	12246	12288	48837	49106	49152	
R_2	2912	3017	3071	3072	12096	12246	12288	48837	49106	49152	
R_3	2912	3017	3071	3072	12096	12246	12288	48837	49106	49152	

Table 1. Theoretical maximum ranks $R_{\rm th}$ of the covariance matrix, for a generic pixelization of the sphere, imposed by the constraints given in the previous section. Different number of pixels ($N_{\rm pix}$) and maximum multipole ($\ell_{\rm max}$) are considered.

$\ell_{\rm max}$ given by the corresponding constraints. Table 1 shows the theoretical maximum ranks achieved by the covariance matrix for different values of $N_{\rm pix}$ and $\ell_{\rm max}$, depending on which symmetries are satisfied. In particular, for all cases, the minimum $\ell_{\rm max}$ necessary to achieve a non-singular matrix (i.e., whose rank is at least as large as $N_{\rm pix}$) is given. To allow for an easier comparison, we have chosen values for $N_{\rm pix}$ equal to the number of pixels of the first resolutions of the `HEALPix` and `Igloo` pixelizations (see sections 4.1 and 4.3 for details). In addition, the constraints imposed by the S_{II} and S_{III} symmetries also depend on the particular number of pixels at $z = 0$. For the sake of simplicity, we have decided this generic pixelization to have the same number of pixels at $z = 0$ as `HEALPix`. As one would expect, including symmetries in the pixelization implies, at least in certain cases, that a higher $\ell_{\rm max}$ is needed in order to achieve a regular covariance matrix.

Although the ranks given in table 1 correspond to the maximum ranks that the covariance matrix can achieve under the presence of the corresponding symmetries, in practice, a specific pixelization may have additional properties or cancellations. This reduces even further the rank for a given multipole, which implies that we need a higher $\ell_{\rm max}$ for this matrix to become regular. In the following subsections we will study the actual rank of the covariance matrix for five specific pixelizations, considering different resolutions. To carry out this analysis, we have calculated numerically the rank of $\mathbf{C}$ using the `MatrixRank` function of the symbolic computation software MATHEMATICA. Hereinafter we will refer to this value as R_N. For comparison, this value is confronted with that obtained from the theoretical constraints, taking into account the symmetries present in each of the considered pixelizations, which we will denote $R_{\rm th}$.

It is worth noting that the particular elements of the covariance matrix depend on the power spectrum of the fluctuations but, according to eq. (2.10), its rank does not (except in the null case of a blank image).[3] This allows us to choose the C_ℓ's and, for the sake of simplicity, in this section we will compute $\mathbf{C}$ for a flat spectrum $C_\ell = 1$. For this simplified

[3]Note also that, in practice, very small values of the power spectrum can introduce numerical errors in the calculation of the rank of $\mathbf{C}$, giving rise to ill-conditioned matrices in cases expected to be non-singular from theoretical arguments (see section 5 for details).

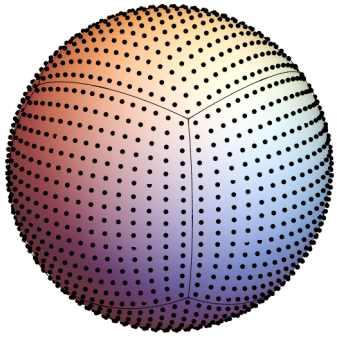

Figure 1. `Cube` pixelization corresponding to res = 5 and $N_{\rm pix} = 1536$.

(res, $N_{\rm pix}$)	(1,6)			(2, 24)				(3,96)									
$\ell_{\rm max}$	2	3	4	2	3	4	5	2	3	4	5	6	7	8	9	10	11
R_N	2	5	6	5	12	19	24	5	12	21	32	45	60	75	88	94	96
$R_{\rm th}$	3	6	6	5	12	19	24	5	12	21	32	45	60	77	92	96	96

Table 2. Numerically calculated rank for the covariance matrix (R_N) compared to the maximum expected theoretical rank ($R_{\rm th}$) for different configurations of the `Cube` pixelization.

case, making use of the addition theorem for spherical harmonics, eq. (2.7) takes the form:

$$\mathbf{C}_{ij} = \sum_{\ell=2}^{\ell_{\rm max}} \frac{2\ell+1}{4\pi} \mathbf{P}_\ell(\mathbf{r}_i \mathbf{r}_j) = \sum_{\ell=2}^{\ell_{\rm max}} \mathbf{P}^\ell(\mathbf{r}_i \mathbf{r}_j). \tag{4.1}$$

As expected, in all the considered cases we have found $R_N \equiv \mathrm{rank}(\mathbf{C}) = \mathrm{rank}(\mathbf{Y})$.

4.1 `Cube`

The `Cube` pixelization [15], represented in figure 1, maps the pixels from the surface of a cube to the unit sphere in such a way that their areas are approximately equal. The successive resolution levels are attained by recursive subdivision of the projected faces of the cube, controlled by the resolution parameter res, which can take positive integer values. The number of pixels is given by $N_{\rm pix} = 6 \times 4^{\rm res-1}$. The minimum resolution, six pixels at the centres of the six faces of the cube, is given by res = 1. This pixelization has been extensively used during the processing of the COBE experiment [20].

In this pixelization all pixels have a S_I-symmetric pixel. They also satisfy the S_{III} symmetry, except for two pixels on the poles for the first resolution level. Table 2 shows the values of the rank of the covariance matrix obtained numerically (R_N) and the maximum theoretical rank ($R_{\rm th}$) as a function of $\ell_{\rm max}$. The pixels of resolutions 2 and 3 satisfy the S_{III} symmetry, thus the maximum theoretical rank is given by R_3. For res = 1, the theoretical ranks have been calculated taken into account that the S_I symmetry is satisfied and that there are two pairs of pixels that also satisfy S_{III}.

The table shows that for some $\ell_{\rm max}$ we have $R_N \leq R_{\rm th}$. In order to understand why the maximum range is not always achieved, let us consider as a workable example the case res = 1, $\ell_{\rm max} = 2$, where we find $R_N = 2$ versus $R_{\rm th} = 3$. For this resolution level we have six

pixels located at $(\pm 1, 0, 0), (0, \pm 1, 0), (0, 0, \pm 1)$ in Cartesian coordinates. Since $\mathbf{C}$ is calculated using the harmonics of $\ell = 2$, $\mathbf{Y}$ is a matrix with 6 rows (number of pixels) and 5 columns (number of harmonics). Following the arguments of the previous section, it is convenient to order the spherical harmonics following the sequence $\{e1, e3, e0, e2\}$ (note that odd values of ℓ are not considered since $\ell_{\rm min} = \ell_{\rm max} = 2$). For our case, this corresponds to an ordering of m of $\{1, -1, 0, -2, 2\}$. Pixels are ordered (0, 0, 1), (1, 0, 0), (0, 1, 0), (-1, 0, 0), (0, -1, 0), (0, 0, -1). In this way, carrying out the corresponding operations, we get the matrix $\mathbf{Y}$:

$$\mathbf{Y} = \begin{pmatrix} 0\ 0 & \frac{\sqrt{\frac{5}{\pi}}}{2} & 0 & 0 \\ 0\ 0 & -\frac{\sqrt{\frac{5}{\pi}}}{4} & \frac{1}{4}\sqrt{\frac{15}{2\pi}} & \frac{1}{4}\sqrt{\frac{15}{2\pi}} \\ 0\ 0 & -\frac{\sqrt{\frac{5}{\pi}}}{4} & -\frac{1}{4}\sqrt{\frac{15}{2\pi}} & -\frac{1}{4}\sqrt{\frac{15}{2\pi}} \\ 0\ 0 & -\frac{\sqrt{\frac{5}{\pi}}}{4} & \frac{1}{4}\sqrt{\frac{15}{2\pi}} & \frac{1}{4}\sqrt{\frac{15}{2\pi}} \\ 0\ 0 & -\frac{\sqrt{\frac{5}{\pi}}}{4} & -\frac{1}{4}\sqrt{\frac{15}{2\pi}} & -\frac{1}{4}\sqrt{\frac{15}{2\pi}} \\ 0\ 0 & \frac{\sqrt{\frac{5}{\pi}}}{2} & 0 & 0 \end{pmatrix}. \tag{4.2}$$

The first two columns of zeros occur because Y_2^1 and Y_2^{-1} contain the product $\sin\theta\cos\theta$, which becomes null for the 6 considered pixels. All points are symmetric in the sense $\mathbf{r} \to -\mathbf{r}$, and therefore we can use eq. (3.2) and transform $\mathbf{Y}$ into a matrix with 3 rows of zeros. Choosing the pixels $(0, 0, 1)$, $(1, 0, 0)$ and $(0, 1, 0)$ when applying the symmetry we get:

$$\mathbf{Y} \to \begin{pmatrix} 0\ 0 & \frac{\sqrt{\frac{5}{\pi}}}{2} & 0 & 0 \\ 0\ 0 & -\frac{\sqrt{\frac{5}{\pi}}}{4} & \frac{1}{4}\sqrt{\frac{15}{2\pi}} & \frac{1}{4}\sqrt{\frac{15}{2\pi}} \\ 0\ 0 & -\frac{\sqrt{\frac{5}{\pi}}}{4} & -\frac{1}{4}\sqrt{\frac{15}{2\pi}} & -\frac{1}{4}\sqrt{\frac{15}{2\pi}} \\ 0\ 0 & 0 & 0 & 0 \\ 0\ 0 & 0 & 0 & 0 \\ 0\ 0 & 0 & 0 & 0 \end{pmatrix}. \tag{4.3}$$

Then, the maximum rank we could ever achieve is 3. Note that $Y_2^2 = Y_2^{-2} = 0$ at $(0, 0, 1)$, so the first row in $\mathbf{Y}_e$ has only one non zero term, at the column that corresponds to Y_2^0. Taking into account that the other two points are S_{III} symmetric, we can get more zero blocks in $\mathbf{Y}_e$. Therefore, the first three rows of the matrix become:

$$\mathbf{Y}_e \to \begin{pmatrix} 0\ 0 & \frac{\sqrt{\frac{5}{\pi}}}{2} & 0 & 0 \\ 0\ 0 & -\frac{\sqrt{\frac{5}{\pi}}}{4} & 0 & 0 \\ 0\ 0 & 0 & -\frac{1}{4}\sqrt{\frac{15}{2\pi}} & -\frac{1}{4}\sqrt{\frac{15}{2\pi}} \end{pmatrix}, \tag{4.4}$$

which yields to a matrix of rank 2, a unit of rank lower than expected taking into account the size of Y_e after applying S_I. The reason for this lower rank for this particular pixelization is that two columns of spherical harmonics, Y_2^{-1} and Y_2^1, are zeros and the columns of Y_2^2 and Y_2^{-2} are equal. This illustrates how in some cases the rank can be lower than expected by the theoretical expressions when computing the rank of matrices $\mathbf{Y}$ calculated on particular sets of pixels.

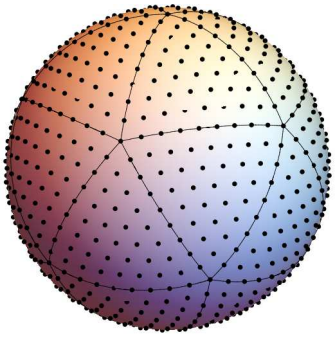

Figure 2. `Icosahedron` pixelization corresponding to res = 5 and $N_{\rm pix}$=812.

(res, $N_{\rm pix}$)	(1, 12)					(2, 92)									
$\ell_{\rm max}$	2	3	4	5	6	3	4	5	6	7	8	9	10	11	12
R_N	5	8	8	11	12	12	21	32	45	60	77	87	88	91	92
$R_{\rm th}$	5	11	12	12	12	12	21	32	45	60	77	90	92	92	92

Table 3. Numerically calculated rank for the covariance matrix (R_N) compared to the maximum expected theoretical rank ($R_{\rm th}$) for different configurations of the `Icosahedron` pixelization.

4.2 `Icosahedron`

The `Icosahedron` pixelization [16], shown in figure 2, is constructed by subdividing the faces of an icosahedron into a regular triangular grid, starting from a first resolution of 12 pixels situated at the vertices of the icosahedron. The pixels are projected onto the sphere in such a way that their areas are approximately equal. Similarly to the `Cube` pixelization, the resolution of the pixelization is controlled by an integer positive parameter res, being the number of pixels given by $N_{\rm pix} = 40 \times {\rm res} \times ({\rm res} - 1) + 12$.

This pixelization satisfies the S_I symmetry. However, since the vertices of the Icosahedron, which are the starting point of the subsequent resolutions, do not fulfil symmetries S_{II} or S_{III}, no further symmetries are expected to be found. In particular, we have tested that this is the case up to resolution res = 9. Table 3 shows the values of the rank of the covariance matrix obtained numerically (R_N) and the maximum theoretically expected range ($R_{\rm th}$) as a function of $\ell_{\rm max}$ for two different resolutions. Note that for the shown resolutions the S_I symmetry is satisfied and, therefore, $R_{\rm th} = R_1$. As for the `Cube` pixelization, $R_N \leq R_{\rm th}$ is always satisfied. The reason why the maximum rank is not always achieved can be easily seen in the lowest resolution (res = 1, $N_{\rm pix} = 12$). If we sum up to $\ell_{\rm max} = 2$, the rank of the matrix is limited by the number of spherical harmonics, which is 5, and we have found $R_N = 5$. If we sum up to $\ell_{\rm max} = 3$, there are 7 new harmonics, thus the rank could increase, in principle, up to 12. However, due to the presence of the S_I symmetry, we have that the maximum theoretical rank is $R_{\rm th} = 11$. Nevertheless, the numerical rank R_N is found to be 8. One of the reasons for the reduction of the rank is that the z-coordinate of all pixels take one of the values $z = \{-1, 1, -\frac{1}{\sqrt{5}}, \frac{1}{\sqrt{5}}\}$ and the Legendre polynomials for $\ell = 3$ and $m = \pm 1$,

$$P_3^{-1}(z) = \frac{1}{8}\sqrt{1-z^2}\left(5z^2-1\right), \qquad P_3^{1}(z) = -\frac{3}{2}\sqrt{1-z^2}\left(5z^2-1\right), \tag{4.5}$$

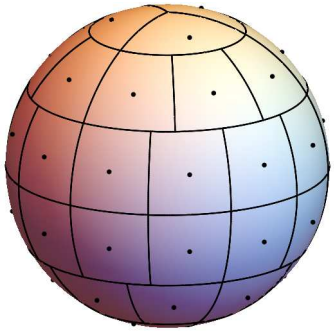

Figure 3. `Igloo` pixelization corresponding to $N_{\rm side}$=2 and $N_{\rm pix}$=48.

happen to cancel at these points, which leads to two zero columns in the $\mathbf{Y}_o$ block. Thus we are left with only five non-zero columns instead of seven for this block, what means that the covariance matrix rank could be ten as maximum. However, due to the particular positions of the pixels in this pixelization scheme, other columns of this block happen to be linearly dependent. In particular, the column that corresponds to $m = 0$ is linearly independent of the other four columns, but the $m = -3$ column is proportional to the $m = -2$ column and the same relation applies to columns $m = 3$ and $m = 2$. Therefore, the rank of the odd block is reduced to 3, and adding up the rank of the even block, which is 5, we finally get rank 8 for the covariance matrix as found. Note that adding multipoles up to $\ell_{\rm max} = 4$ does not change the situation, but going up to $\ell_{\rm max} = 5$ raises the rank to 11. Finally, adding multipoles up to $\ell_{\rm max} = 6$ provides enough independent columns to get a non-singular covariance matrix.

4.3 `Igloo`

The `Igloo` pixelation [17] divides the sphere in bands which are perpendicular to the axis z in variable intervals of θ. Each band is divided into a different number of pixels at constant intervals of ϕ, and the interval varies from band to band. Thus, the edges of the pixels are of constant latitude and longitude. Among the different options, the one presented here consists of a base resolution of twelve pixels, three on each of the poles and six on the central band. The angles have been chosen in such a way that the resultant pixels are of equal area. The subsequent resolutions were obtained by recurrent subdivisions of each pixel into other four pixels of equal area, always having three pixels at each pole.

The number of pixels is $N_{\rm pix} = 12 \times N_{\rm side}^2$. The resolution is controlled by the $N_{\rm side}$ parameter, which can take as values integers that are a power of 2. Figure 3 shows the `Igloo` pixelization for $N_{\rm side} = 2$. The Igloo pixels are symmetric in the S_I sense. Moreover, for all resolutions there are couples of S_{II}-symmetric pixels in the central area. For resolutions 2 and higher, there are also some pixels with S_{III} symmetry. Taking into account these particular symmetries, we find that $R_N = R_{\rm th} = R_1$ for all $\ell_{\rm max}$ for resolutions $N_{\rm side} = \{1, 2\}$. For $N_{\rm side} \geq 4$ the numerical rank of the covariance matrix is found to be smaller than the maximum theoretical rank in some cases. Table 4 shows the results for $N_{\rm side} = 4$ and different values of $\ell_{\rm max}$.

$(N_{\rm side}, N_{\rm pix})$	(4, 192)														
$\ell_{\rm max}$	2	3	4	5	6	7	8	9	10	11	12	13	14	15	16
R_N	5	12	21	32	45	60	77	96	117	140	162	179	187	191	192
$R_{\rm th}$	5	12	21	32	45	60	77	96	117	140	165	186	192	192	192

Table 4. Numerically calculated rank for the covariance matrix (R_N) compared to the maximum expected theoretical rank ($R_{\rm th}$) for different configurations of the `Igloo` pixelization.

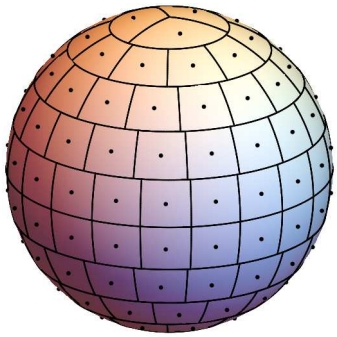

Figure 4. `GLESP` pixelization corresponding to a resolution parameter $N = 10$. In this figure the rings have been rotated to make the pixels S_I-symmetric.

4.4 `GLESP`

The Gauss-Legendre Sky Pixelization (`GLESP`) [18] (figure 4) makes use of the Gaussian quadratures to evaluate numerically the integral with respect to z of the expression:

$$a_{\ell m} = \int_{-1}^{1} dz \int_{0}^{2\pi} d\phi \Delta T(z,\phi) Y^*_{\ell m}(z,\phi), \tag{4.6}$$

which can be formally expressed with this method in an exact form as a weighted finite sum. The surface of the sphere is divided into N rings of trapezoidal pixels with values of θ at the centres of the pixels according to the Gauss-Legendre quadrature method. There is some degree of freedom to fix the number and size of the pixels on the rings, but preferentially they are defined to make the equatorial ones roughly square. The number of pixels on the rest of the rings is chosen in such a way that all the pixels have nearly equal area.[4] Finally, polar pixels are triangular. Note that this pixelization is not hierarchical.

Regarding the presence of symmetries, those pixels belonging to rings which have been divided into a number of pixels which is a multiple of two or four will satisfy S_{II} or S_{III}. However, this is not always the case and, therefore, the `GLESP` pixelization does not fulfil these symmetries as a whole. Referring to the S_I-symmetry, it can be fulfilled in certain cases if the rings are rotated with respect to the z axis (note that this rotation that does not

[4]It is interesting to note that to study the CMB polarization and with the aim of obtaining a better evaluation of the ${}_{0,\pm2}a_{\ell,m}$-coefficients, two additional over-pixelization versions of this scheme have been proposed [21]. In this case, there is a larger number of pixels on the rings than in the nearly equal area scheme considered in this paper, with decreasing area of the pixels on the rings as they get closer to the polar caps. Since our work is oriented to the scalar field case, we will study the nearly equal area version of the pixelization.

$(N, N_{\rm pix})$	(4, 22)				
$\ell_{\rm max}$	2	3	4	5	6
R_N	5	12	17	21	22
$R_{\rm th}$	5	12	18	22	22

Table 5. Numerically calculated rank for the covariance matrix (R_N) compared to the maximum expected theoretical rank ($R_{\rm th}$) for the GLESP pixelization for $N = 4$.

change the essence of the pixelization). In particular, if the number of rings is even, each of the rings on one hemisphere can be positioned with respect to the opposite ring on the other hemisphere in such a way that the S_I-symmetry is satisfied. If N is an odd number, there is an unmatched ring on the equator, and the symmetry is only fulfilled if this ring is divided into an even number of pixels. Fig. 4 shows the GLESP pixelization for $N = 10$ in a S_I-symmetric configuration.

Table 5 shows the values of the rank for the case with 4 rings. The number of pixels is 22, 8 on each of the central rings and 3 on each of the poles. For the sake of simplicity and in order to allow for a better comparison with the other considered pixelizations, we have rotated the rings in such a way that all the pixels have their S_I-symmetric pair. The pixels on the two central rings have a S_I, S_{II} and S_{III}-symmetric partner, but the pixels on the poles do not have a S_{II} and S_{III}-symmetric one. In this situation, the R_{II} and R_{III} expressions are not strictly valid. However, if we find that $R_I = R_{II} = R_{III}$, i.e., that the matrix rank is not reduced under the presence of S_{II} and S_{III}, we can conclude that the same is valid when the symmetries are only partially fulfilled, as for the GLESP pixelization. For the considered case, we have indeed found $R_I = R_{II} = R_{III}$ for all the values of $\ell_{\rm max}$. Table 5 shows that for $\ell_{\rm max} = 4$ and $\ell_{\rm max} = 5$ the rank of $\mathbf{C}$ is one unit lower than the theoretical rank. Let us try to explain where this unit is lost. Since the S_I-symmetry is fulfilled, we have two diagonal blocks in $\mathbf{Y}$. For $\ell_{\rm max} = 4$, the block of odd ℓ has 11 rows and 7 columns, and its rank is 7. The block of even ℓ, 11 rows and 14 columns, and its rank is 10. Due to the way in which the values of θ are chosen in this pixelization scheme, the roots of the Legendre polynomial with $\ell = 4$ in the case of $N = 4$, the column of $\mathbf{Y}$ that corresponds to the harmonic $Y_{4,0}$ is made up of zeros. Aside from this column, among the other 13 columns there are only 10 linearly independent columns. We have found that the group of ten that corresponds to the five harmonics of values of $\ell = 2$ and the other five of $\ell = 3$ and values of m : -4, -3, -1, 1 and 3 are linearly independent. When $\ell_{\rm max} = 5$, we get 11 new columns on the odd block of $\mathbf{Y}$, and the rank in this block saturates to 11, but the block of even ℓ still has 11 rows and 14 columns but only 10 linearly independent columns; thus the rank is a unit lower than the theoretical value. When $\ell_{\rm max} = 6$ we get new linearly independent columns in the block of even ℓ, and the rank saturates.

4.5 HEALPix

The most extensively used pixelization for CMB analysis is HEALPix, which stands for Hierarchical Equal Area iso-Latitude Pixelization [19]. HEALPix divides the sphere into twelve spherical diamond-shaped pixels on three rings, one of them on the equator and the other two towards the poles. The four pixels forming each ring have the same latitude and each diamond is then subdivided recursively in order to get the pixels for the different resolution levels. The total number of pixels is $N_{\rm pix} = 12 \times N_{\rm side}^2$, where $N_{\rm side}$ is the resolution pa-

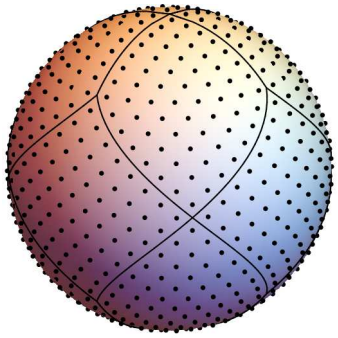

Figure 5. `HEALPix` pixelization corresponding to $N_{\rm side} = 8$ and $N_{\rm pix}$=768.

$(N_{\rm side}, N_{\rm pix})$	(8, 768)			
$\ell_{\rm max}$	25	26	27	28
R_N	672	724	760	768
$R_{\rm th}$	672	725	761	768

Table 6. Numerically calculated rank for the covariance matrix (R_N) compared to the maximum expected theoretical rank ($R_{\rm th}$) for the `HEALPix` pixelization for $N_{\rm side} = 8$ in the multipole regime in which $\mathbf{C}$ becomes regular.

rameter, which is always an integer power of 2. Figure 5 shows the `HEALPix` pixelization for $N_{\rm side}$=8. By construction all the pixels satisfy the S_I, S_{II} and S_{III} symmetries. We find that for the three lowest resolutions ($N_{\rm side} = 1, 2$ and 4), the covariance matrix always achieve the maximum possible rank, i.e., $R_N = R_{\rm th} = R_3$ for all $\ell_{\rm max}$. The first reduction of rank occurs for $N_{\rm side} = 8$ and $\ell_{\rm max} = 26$ (see table 6). In particular, when $\ell_{\rm max} = 26$ we have $R_{\rm th} = 725$ and $R_N = 724$. Let us focus on this case in more detail. We have found that the loss of rank of the covariance matrix is found to lie in block $\mathbf{Y}_{e2}$. The number of rows in block $\mathbf{Y}_{e2}$ is determined by the quantity $k/4 + u/2$, while the number of columns is given by the number of spherical harmonics with even ℓ and $mod(m, 4) = 2$ (see appendix D for details). In particular, for $N_{\rm side} = 8$ we have a total of 768 pixels. Among these, 32 have $z = 0$, one half of them with $0 \leq \phi < \pi$ (i.e. $u = 16$). We also have 368 pixels with $z > 0$ (i.e. $k = 368$). Therefore, the block $\mathbf{Y}_{e2}$ has $k/4 + u/2 = 100$ rows. For $\ell_{\rm max} = 26$, the number of spherical harmonics with ℓ even and $mod(m, 4) = 2$ is 98. So the block has size 100×98, but rank 97. We have also checked that the rank of all the sub-blocks that can be formed by removing any particular column of $\mathbf{Y}_{e2}$ is 97. This means that any group of 97 out of the 98 spherical harmonics are linearly independent, but the 98 columns taken as a whole are linearly coupled. This shows, again, how some units of rank can be lost by properties related to the particular values of the pixels of the chosen pixelization.

So far we have demonstrated, for five different pixelization schemes, that for a given resolution parameter, it is possible to determine the lowest $\ell_{\rm max}$ needed to make $\mathbf{C}$ regular. Furthermore, a detailed analysis of the pixel properties allows us to detect linear combinations of spherical harmonics that lead to reductions of the maximum theoretical rank. When this happens, it is necessary to raise $\ell_{\rm max}$ in order to regain regularity.

Among the five pixelization schemes we have considered, HEALPix is particularly interesting because of two nice properties. On the one hand, from the tests we have presented, it seems to be the pixelization in which the reduction of the rank of the covariance matrix with respect to the maximum expected theoretical value is lower. On the other hand, since it presents the three types of considered symmetries for all the resolution levels, it is easy to divide the $\mathbf{Y}$ matrix into eight blocks, which in turn makes it easier to study the linear independence of the columns of the matrix. For these reasons, together with the fact that HEALPix is the most commonly used pixelization for CMB analysis, we will only consider this pixelization along the rest of the paper.

The discussion so far has focused on an idealized case. In particular, there is a number of real life issues we have not taken into account yet:

- Until now we have used $C_\ell = 1$ and neglected the window function B_ℓ.
- In many real life applications $\mathbf{C}$ is calculated for a masked area of the sky.
- We have not considered the effect of noise.

We will discuss the impact of these effects on the regularity of $\mathbf{C}$ in the next sections.

5 Effect of the power spectrum and the beam transfer function

Up to now we have studied the rank of $\mathbf{C}$ according to eq. (2.7) using a simplified angular power spectrum $C_\ell = 1$. In a realistic CMB analysis, we would use the correspondent C_ℓ's and the beam transfer function B_ℓ which encodes the response of the beam of the experiment. Therefore:

$$\mathbf{C}_{ij} = \sum_\ell \frac{2\ell+1}{4\pi} C_\ell B_\ell^2 \mathbf{P}_\ell(\mathbf{r}_i \mathbf{r}_j). \tag{5.1}$$

The beam transfer function usually drops quickly for high multipoles and the sum of eq. (5.1) is dominated by low-ℓ terms. As we mentioned before, theoretically this should not affect the rank of $\mathbf{C}$. However, in practice, since the sums are computed numerically, it is possible that the regularity of $\mathbf{C}$ is affected by machine precision limitations. In table 7 we compare the rank of $\mathbf{C}$ as calculated in the previous section (i.e. C_ℓ=1 for all multipoles and not including any window function) with that calculated using a realistic CMB power spectrum, for the HEALPix pixelization with resolution $N_{\rm side} = 8$. In particular, we have considered the Planck ΛCDM best-fit model that includes also information from the Planck lensing power spectrum reconstruction and Baryonic Acoustic Oscillations [22],[5] a Gaussian beam with a FWHM corresponding to 2.4 times the pixel size at the considered resolution (FWHM=17.6 degrees for $N_{\rm side} = 8$) and we have also taken into account the corresponding HEALPix pixel window function. This model will be used along the paper, unless otherwise stated. As before, we have estimated the rank of the covariance matrix using MATHEMATICA with its default machine precision (which corresponds to the standard double precision). From the results of table 7, we see that the rank estimated for the covariance matrix can be significantly smaller when working under realistic conditions for the power spectrum, indicating that numerical errors may have an important effect in real life applications. We can further study the effect

[5] More specifically we have used model 2.30 described in the document https://wiki.cosmos.esa.int/planckpla2015/images/f/f7/Baseline_params_table_2015_limit68.pdf from the Planck Explanatory Supplement

$\ell_{\rm max}$	24	25	26	27	28	29	30	31
$R_N(1)$	621	672	724	760	768	768	768	768
$R_N(2)$	621	671	709	735	752	761	766	768

Table 7. Numerically calculated ranks of $\mathbf{C}$ for a `HEALPix` resolution of $N_{\rm side} = 8$ and different values of $\ell_{\rm max}$. $R_N(1)$ is the rank of $\mathbf{C}$ using $C_\ell = 1$ and not including any beam window function. $R_N(2)$ is the rank of the same matrix when considering a realistic CMB power spectrum and beam.

$\ell_{\rm max}$	Machine	50	200	400	800
26	-7.70×10^{-615}	2.95×10^{-2713}	-2.49×10^{-9329}	1.44×10^{-18046}	1.05×10^{-35734}
27	-9.50×10^{-390}	-4.58×10^{-759}	4.90×10^{-1979}	-1.74×10^{-3545}	-4.80×10^{-6767}
28	6.91×10^{-255}	3.12×10^{-256}	3.12×10^{-256}	3.12×10^{-256}	3.12×10^{-256}
29	1.64×10^{-174}	2.62×10^{-174}	2.62×10^{-174}	2.62×10^{-174}	2.62×10^{-174}
30	5.54×10^{-136}	5.66×10^{-136}	5.66×10^{-136}	5.66×10^{-136}	5.66×10^{-136}
31	4.39×10^{-122}	4.40×10^{-122}	4.40×10^{-122}	4.40×10^{-122}	4.40×10^{-122}

Table 8. Determinant of $\mathbf{C}$ with different precisions and $\ell_{\rm max}$.

of numerical precision on the effective rank of $\mathbf{C}$ by means of the MATHEMATICA software. MATHEMATICA can operate the sums of spherical harmonics symbolically and convert the result into numerical format with any desired number of decimals. Those quantities which are available with a limited precision (e.g. the power spectrum or the pixel window function) can be rationalized in MATHEMATICA, which helps to control the propagation of numerical errors.[6] In this way, calculating the covariance matrix given by eq. (5.1) with a precision of 200 decimals we recover the ranks given by $R_N(1)$ in table 7. This confirms that the loss of rank observed in table 7 is in fact a matter of numerical errors.

The effect of numerical precision can be observed in more detail in table 8. We have calculated the determinant of $\mathbf{C}$ for a realistic power spectrum for different values of $\ell_{\rm max}$ and different numerical precisions: the machine native precision and 50, 100, 200, 400 and 800 decimals. For $\ell_{\rm max} = 26$ and $\ell_{\rm max} = 27$ the determinant must be zero because the theoretical rank is lower than 768. This fact is easily seen at higher numerical precisions, where the value of the determinant quickly drops to zero. Conversely, at $\ell_{\rm max} = 28$, 29 and 30, the determinant is non-zero, and, even if very small, we see that its value is stable when sufficiently high precision is used. In particular, the default machine precision is not enough to get the correct value of the determinant (considering a precision of two decimal places), although it gets closer to the correct value as $\ell_{\rm max}$ increases. This relates to our previous finding showing that the estimated rank is lower than expected for these values of $\ell_{\rm max}$ when using the default machine precision, and it becomes correct for higher numerical precisions.

6 Effect of noise

Another common complexity on CMB data is the presence of instrumental noise. Let us now consider the effect of adding a zero mean noise $\mathbf{n}$ to the signal $\mathbf{s}$. Given that noise and signal are expected to be statistically independent, the covariance matrix of the data $\mathbf{x} = \mathbf{s} + \mathbf{n}$ is simply given by the sum of the signal ($\mathbf{S}$) and noise ($\mathbf{N}$) covariance matrices. Moreover, if

[6] Of course this comes at the cost of increasing the computational time.

$N_{\rm side}$	$N_{\rm pix}$	$l_{\rm max}$	$\mathbf{S}_{ii}$	No noise	$f_n = 9.5$	9.0	8.5	8.0	7.5	7.0
4	192	14	487	**192**	192	192	192	192	192	192
8	768	28	1057	752	752	756	**768**	768	768	768
16	3072	56	1655	2937	2937	2937	2938	**3072**	3072	3072
32	12288	111	2308	11518	11518	11518	11518	11518	**12288**	12288

Table 9. Rank (R_N) of $\mathbf{C}$ for several `HEALPix` resolutions after adding different levels of noise. The columns show, from left to right: the resolution parameter, the corresponding number of pixels, the $\ell_{\rm max}$ used for the calculation of $\mathbf{C}$ (which is the theoretical multipole that makes the matrix regular), the value of the diagonal element $\mathbf{S}_{ii}$ (i.e. the CMB variance, in units of $(\mu{\rm K})^2$), the matrix rank without noise and the one obtained after adding noise with different values of the f_n parameter such that $\sigma^2 = 10^{-f_n}$. The bold face indicates the level of noise at which the matrix $\mathbf{C}$ becomes regular.

the noise is not spatially correlated, the matrix $\mathbf{N}$ is diagonal. In that case:

$$\mathbf{C}_{ij} = \mathbf{S}_{ij} + \mathbf{N}_{ij} = \sum_{\ell=\ell_{\rm min}}^{\ell_{\rm max}} \frac{2\ell+1}{4\pi} C_\ell B_\ell^2 \mathbf{P}_\ell(\mathbf{r}_i \mathbf{r}_j) + \sigma_i^2 \delta_{ij}. \tag{6.1}$$

Taking into account that each column of $\mathbf{C}$ is given by the sum of two columns, we can expand by columns its determinant. In this way, the expansion takes the form of the sum of 2^n determinants, one of them containing only columns from $\mathbf{S}$, a second one containing only columns from $\mathbf{N}$ and the rest containing columns from both matrices. The determinants that contain columns from $\mathbf{S}$ can be either positive or null, depending on the value of $\ell_{\rm max}$ and the pixel configuration, but the term that depends only on columns from $\mathbf{N}$ is always positive. It can also be easily shown that the terms with columns from both matrices are also greater or equal than zero. Therefore, we have:

$$\det \mathbf{C} \geq \det \mathbf{N} > 0. \tag{6.2}$$

This shows that the presence of noise regularizes the covariance matrix. This is a well known fact, and in many applications it is common to use a small amount of artificial noise to help regularizing a numerically ill-behaved covariance matrix [5, 23]. The question arising in these cases is what is the optimal noise level to be introduced in order to make the matrix regular without degrading too much the quality of the data.

We have carried out some tests in order to illustrate the regularizing effect of adding noise to the covariance matrix for four different resolutions ($N_{\rm side} = 4$, 8, 16 and 32) of the `HEALPix` pixelization. We have used the same Planck ΛCDM model as in the previous section for the CMB power spectrum and a Gaussian beam with FWHM equal to 2.4 times the pixel size at each resolution. The pixel window function given by `HEALPix` has also been taken into account. For each case we have performed the summations up to the $\ell_{\rm max}$ value for which $\mathbf{C}$ is regular according to the constraint R_3. We have also added different levels of isotropic white noise according to $\sigma^2 = 10^{-f_n}$ $(\mu{\rm K})^2$, to be compared with the CMB variance given in the fourth column of table 9. As in the previous section, the rank of the covariance matrix for each of the considered cases has been obtained using MATHEMATICA with its default machine precision and is given in table 9.

We find that for $N_{\rm side} = 4$, the covariance matrix is regular even without the presence of noise, whereas for higher resolutions it becomes necessary to add a certain level of noise

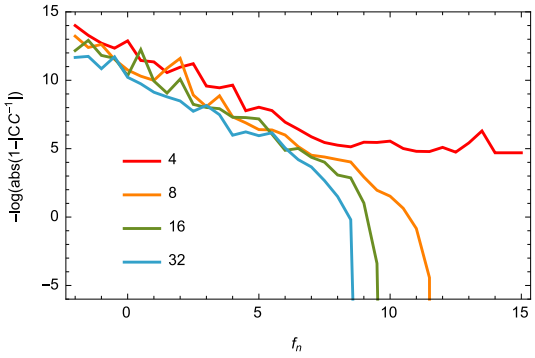

Figure 6. Measurement of the departure of the numerical value of $|\mathbf{C}\mathbf{C}^{-1}|$ from unity versus the level of added noise, for $N_{\rm side}$= 4, 8, 16 and 32 (see text for details).

for the matrix to be regular. Note that the required level of noise grows with $N_{\rm side}$, although it is always very small in comparison to the value of the CMB variance and, therefore, it is not expected to compromise the quality of the data.

In many scientific applications, as for example the estimation of the power spectrum through the Quadratic Maximum Likelihood method [2], it is necessary to perform operations with $\mathbf{C}$ or its inverse. Such operations propagate numerical errors and may lead to instabilities even if one starts with a regular matrix. In figure 6 we show the result of the operation $-\log\left(\mathrm{abs}\left(1-|\mathbf{C}\mathbf{C}^{-1}|\right)\right)$, with $\mathbf{C}$ calculated using the theoretical $\ell_{\rm max}$ value that makes the matrix regular (third column in table 9), as a function of the noise level. Positive values of this quantity indicate approximately the decimal place at which the determinant $|\mathbf{C}\mathbf{C}^{-1}|$ departs from unity, while negative values show how many orders of magnitude this determinant (in absolute value) is greater than unity. This gives an indication of the level of noise required to operate with the covariance matrix and its inverse within the required precision.

7 Effect of masking

The first effect of masking is a reduction of the number of pixels over which the covariance matrix is computed, and therefore a smaller dimension of $\mathbf{C}$. Consequently, a lower value of $\ell_{\rm max}$ will be needed in general to obtain a regular matrix. A second more subtle effect is the possible breaking of pixel – spherical harmonic symmetries. In section 3 we studied the effect of three kind of symmetries, S_I, S_{II} and S_{III}. We showed that, among them, S_I has the greatest impact on the rank of the covariance matrix. Therefore, for the sake of simplicity, in this section we will study the effect of masking only under the presence of the S_I symmetry.

Let us consider that, for a fixed resolution parameter and a given mask geometry, we have n valid pixels. Let us also consider that, among these pixels, n_p have their symmetric pixel inside the region allowed by the mask, while n_u pixels do not have it. Taking into account the symmetries of the n_p pixels the matrix $\mathbf{Y}$ can be transformed as described in

section 3:

$$\mathbf{Y} \rightarrow \begin{pmatrix} \mathbf{Y}^{even}_{n_p/2\times N_e} & \mathbf{0}_{n_p/2\times N_o} \\ \mathbf{0}_{n_p/2\times N_e} & \mathbf{Y}^{odd}_{n_p/2\times N_o} \\ \mathbf{Y}^{even}_{n_u\times N_e} & \mathbf{Y}^{odd}_{n_u\times N_o} \end{pmatrix}, \tag{7.1}$$

where, for example, $\mathbf{Y}^{even}_{n_p/2\times N_e}$ stands for a block with $n_p/2$ rows and N_e columns, whose elements are the spherical harmonics of even ℓ calculated over the independent half of symmetrical pixels inside the mask. For the matrix of eq. (7.1) to be invertible (see appendix E for details), it is necessary that

$$N_e \geq n_p/2, \quad N_o \geq n_p/2, \tag{7.2}$$

due to the pixel symmetry, and

$$N_e + N_o \geq n_p + n_u, \tag{7.3}$$

so that there are at least as many spherical harmonics as pixels. The previous expressions allow us to find the minimum $\ell_{\rm max}$ that makes the matrix regular in a case with mask and S_I symmetry.

We can also calculate the maximum rank of a matrix given the number of pixels, the mask, the number of pixels with and without a symmetric partner and the value of $\ell_{\rm max}$. Transforming the matrix of eq. (7.1) into diagonal blocks, in appendix E we show that the rank matrix is constrained by:

$$\mathrm{rank}(\mathbf{Y}) \leq \min(n_p/2, N_e) + \min(n_p/2, N_o) + \min(n_u, L), \tag{7.4}$$

were $L = N_e - \min(n_p/2, N_e) + N_o - \min(n_o/2, N_e)$. The expression (7.4), R_M hereafter, generalizes expression (3.4) for any mask configuration.

As an example, let us consider the case of $N_{\rm side} = 8$ in the `HEALPix` pixelization and the mask produced by the `SEVEM` component separation method [10] corresponding to the first *Planck* data release.[7] The `SEVEM` mask removes 154 pixels of the sky at this resolution level. Among the 614 remaining pixels, 590 have a S_I symmetrical pixel, whereas 24 do not have a symmetrical partner. Figure 7 shows the locations of paired and unpaired pixels for this case.

Table 10 shows the maximum expected rank $R_{\rm th}$ of the covariance matrix according to R_M and those calculated with MATHEMATICA using a realistic CMB power spectrum and beam (R_N). In addition, two different precisions are considered: the native precision of the machine and a 100-digit precision. We find that the rank estimated with MATHEMATICA coincides in all the considered cases with the maximum allowed theoretical rank when using the higher precision, whereas numerical errors affect the calculation using the default precision.

8 Application to the QML method

As an example of application of the discussion above, let us consider the Quadratic Maximum Likelihood (QML) method [2, 24, 25] introduced for the estimation of the angular power spectrum. Different applications of the QML have been carried out to obtain the CMB temperature and polarization power spectrum (e.g. [5, 26]) as well as the cross-correlation between the CMB and the Large Scale Structure through the Integrated Sachs Wolfe effect

[7] All Planck products are publicly available at the Planck Legacy Archive, `http://pla.esac.esa.int/pla`

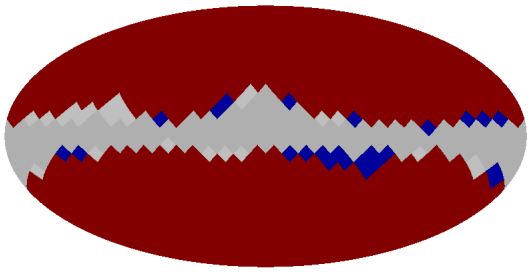

Figure 7. Location of the pixels outside the SEVEM mask for $N_{\rm side} = 8$. The pixels allowed by the mask with an S_I symmetrical partner are red, while those without a symmetric partner are blue. The light and dark grey pixels are discarded by the mask. In particular, the light grey pixels show the points symmetrical to the unpaired blue ones.

$l_{\rm max}$	21	22	23	24	25	26
$R_{\rm th}$	480	525	572	614	614	614
R_N (default)	480	525	571	602	611	614
R_N (100)	480	525	572	614	614	614

Table 10. Rank of $\mathbf{C}$ for the HEALPix pixelization at the $N_{\rm side} = 8$ resolution using the SEVEM mask for different values of $\ell_{\rm max}$. $R_{\rm th}$ is the maximum theoretical rank according to R_M, and R_N is the rank of $\mathbf{C}$ calculated with MATHEMATICA using the default and 100-digit precisions.

[27]. The QML method gives unbiased, minimum variance estimator of the CMB angular power spectrum, $\widehat{D}_\ell = \ell(\ell+1)\widehat{C}_\ell/2\pi$, of a map $\mathbf{x}$ by means of a quadratic estimator. The power can be computed through the following quantity y_ℓ:

$$y_\ell = \frac{1}{2}\frac{B_\ell^2}{\ell(\ell+1)/2\pi}\mathbf{x}^t\mathbf{C}^{-1}\mathbf{P}^\ell\mathbf{C}^{-1}\mathbf{x} - n_\ell, \tag{8.1}$$

where B_ℓ takes into account the effect of the beam as well as the pixel window function, n_ℓ is a correction term that removes the noise bias and the matrix $\mathbf{P}^\ell$ is defined in eq. (4.1). The power in y_ℓ is a linear combination of the *true* power of the map:

$$y_\ell = \sum_{\ell'} \mathbf{F}_{\ell\ell'} D_{\ell'}, \tag{8.2}$$

where $\mathbf{F}$ is the Fisher matrix computed in terms of the parameters D_ℓ. If $\mathbf{F}$ is regular, an estimator of $\widehat{D}_\ell$ can be defined as:

$$\widehat{D}_\ell = \sum_{\ell'} \mathbf{F}^{-1}_{\ell\ell'} y_{\ell'}. \tag{8.3}$$

As seen from eq. (8.1), the estimator requires the inverse of the covariance matrix $\mathbf{C}$ and therefore the performance of the QML method depends critically on the regularity of that matrix.

As a working example, let us consider the case of HEALPix pixelization at resolution $N_{\rm side} = 32$ and full-sky. The total number of pixels is 12288 and, according to the theoretical values given in table 1, it is necessary to sum up to $\ell_{\rm max} = 111$ in order to get the maximum

rank of $\mathbf{C}$. However, from table 9 we know that with this $\ell_{\rm max}$ the numerical matrix is not regular. A solution for this problem is to add a *small* amount of noise to make $\mathbf{C}$ regular. However, what does *small* mean in this context? If the artificial noise is too large, the performance of the QML method will suffer degradation, particularly at high multipoles, but if the noise level is too small the matrix will pose numerical instabilities. Therefore the choice of the correct noise level is not trivial. In this section we will study in detail the effect of noise addition and investigate the optimal *small* amount of noise to be added.

In particular, we will study the value of the determinant $|\mathbf{C}\mathbf{C}^{-1}|$, the statistical properties of the product $\eta = \mathbf{x}^t\mathbf{C}^{-1}\mathbf{x}$ (which, since both the simulated CMB and noise are Gaussian, should follow a χ^2 distribution with the same number of degrees of freedom as of pixels in the map), and the estimation and error bar of the power spectrum given by the QML method after the addition of different levels of noise. In order to do this, we first compute the matrix $\mathbf{S}$ in eq. (6.1) using the Planck best-fit model (and including the beam and pixel window function) with $\ell_{\rm max} = 111$ and secondly we add isotropic white noise with variance $\sigma^2 = 10^{-f_n}$; CMB maps are then simulated with the `HEALPix` package at $N_{\rm side} = 32$, and noise is added following a normal distribution with dispersion parameterised by f_n.

Table 11 shows the value of the determinant $|\mathbf{C}\mathbf{C}^{-1}|$ (fifth column) for different levels of regularizing noise as well as the quantity $-\log\left(\mathrm{abs}\left(1-|\mathbf{C}\mathbf{C}^{-1}|\right)\right)$ (sixth column), introduced in section 6. It is apparent that for very low levels of noise, the covariance matrix becomes singular and the determinant produces values which are very far from unity. Conversely, for values of $f_n \lesssim 5$, the determinant departs from its theoretical value approximately in the sixth decimal place (or even better). Note that $f_n = 5$ corresponds to a very small level of noise compared to the signal (second column) and, therefore, it is not expected to imply a degradation of the data. Of course, the more noise we include, the closer the determinant gets to unity, but at the price of degrading the data.

The product $\eta = \mathbf{x}^t\mathbf{C}^{-1}\mathbf{x}$ should follow a χ^2 distribution with 12288 degrees of freedom. However, if there are numerical instabilities in $\mathbf{C}^{-1}$, this quantity will depart from its theoretical distribution. In figure 8 we show two histograms of η obtained from 10000 simulations of CMB plus noise with two different levels of noise in comparison with the expected χ^2 distribution. The $f_n = 5$ noise results in a regular covariance matrix, and $f_n = 9.25$ is in the limit in which the tests fail dramatically. It clearly shows how the distribution of η departs from the theoretical distribution when the level of the noise is low. This can be quantified, for instance, by applying the Cramér-von Mises goodness-of-fit hypothesis test [28], which determines the p-value of the data to be consistent with the theoretical distribution. The p-values obtained for the different considered cases are given in table 11 (fourth column). As one would expect, the data are consistent with a χ^2 distribution only when the covariance matrix is regularized by adding a certain level of noise to the simulated data.

So far, we have studied two generic statistics directly related to the covariance matrix. We will now investigate how the possible singularity of $\mathbf{C}$ propagates through the QML estimator. Figure 9 shows the average and 1σ error for $\widehat{D}_\ell$ when considering three different levels of regularizing noise, namely, $f_n = 0$, 5 and 9.25. If the noise level is too small, the estimation of the low multipoles is systematically biased downwards. If the noise is too high, the performance of the estimator degrades at high ℓ and the error bars grow quickly. At intermediate noise levels, the estimator is unbiased and the performance of the method is basically limited only by cosmic variance, up to $\ell \approx 3N_{\rm side}$.

To further quantify the performance of the QML method under the presence of different

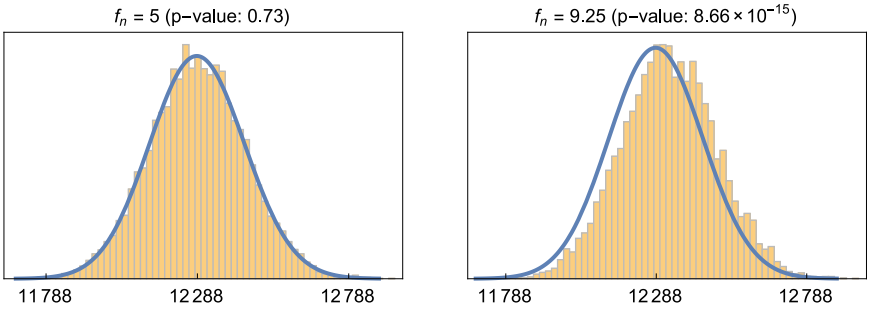

Figure 8. Distribution of numerical values of $\mathbf{x}^t\mathbf{C}^{-1}\mathbf{x}$ compared with the theoretical distribution, for noise levels $f_n = 5$ and 9.25 obtained from 10000 simulations.

levels of regularizing noise, we have calculated the following quantity:

$$\left\langle \frac{\sigma_\ell^{QML}}{\sigma_\ell^{CV}} \right\rangle = \frac{1}{3N_{\rm side}-1} \sum_{\ell=2}^{3N_{\rm side}} \frac{\sigma_\ell^{QML}}{\sigma_\ell^{CV}}, \tag{8.4}$$

where σ_ℓ^{QML} corresponds to the dispersion of the QML estimator and σ_ℓ^{CV} to that inferred from the cosmic variance. This average ratio gives information on how much the error in the estimation of the QML degrades with respect to the optimal case. Table 11 shows this ratio for different levels of added noise. For a very low level of noise, the performance of the estimator is clearly degraded due to the singularity of $\mathbf{C}$, while for a high level of noise, its effect in increasing the error of the estimator at high multipoles also becomes apparent. There is an intermediate region at which the error in the estimation is very close to the error expected by cosmic variance, i.e., $\langle \sigma_\ell^{QML}/\sigma_\ell^{CV} \rangle \approx 1$.

By looking simultaneously at the results for the three previous tests, we can get a better idea of which is the optimal level of noise to be added in order to regularize the covariance matrix without degrading the data for the particular case studied in this section. The hypothesis test based on $\mathbf{x}^t\mathbf{C}^{-1}\mathbf{x}$ and the determinant $|\mathbf{C}\mathbf{C}^{-1}|$ probe similar properties, since both of them focus directly on the inverse of $\mathbf{C}$. As one would expect, the values in table 11 show that the results from both statistics are consistent. In particular, when the noise is high, both tests show that the covariance matrix is regular, while, when the noise is reduced, the determinant departs from unity and the p-value of the Cramér-von Mises test gets close to zero. Note that the more noise is added, the better the discriminant is, but this does not indicate the level of noise at which the quality of the data starts to get compromised. Therefore, it is necessary to look at other complementary statistics (such as the one based on the QML method) in order to find the appropriate range of noise, sufficiently high as to regularize the covariance matrix but also as low as possible so that the data is not degraded. By studying the error bar in the estimation of the power spectrum with QML with respect to that expected by cosmic variance, we find that very low values of regularizing noise ($f_n = 9$) can give an apparent good result in this test but a bad value for the determinant. Thus, for the sake of consistency and being conservative, one should choose a value of noise that achieves both a good value for the determinant and a minimum error for the QML method. In this sense, table 11 shows that values of f_n between 3 and 5 are the most appropriate; the

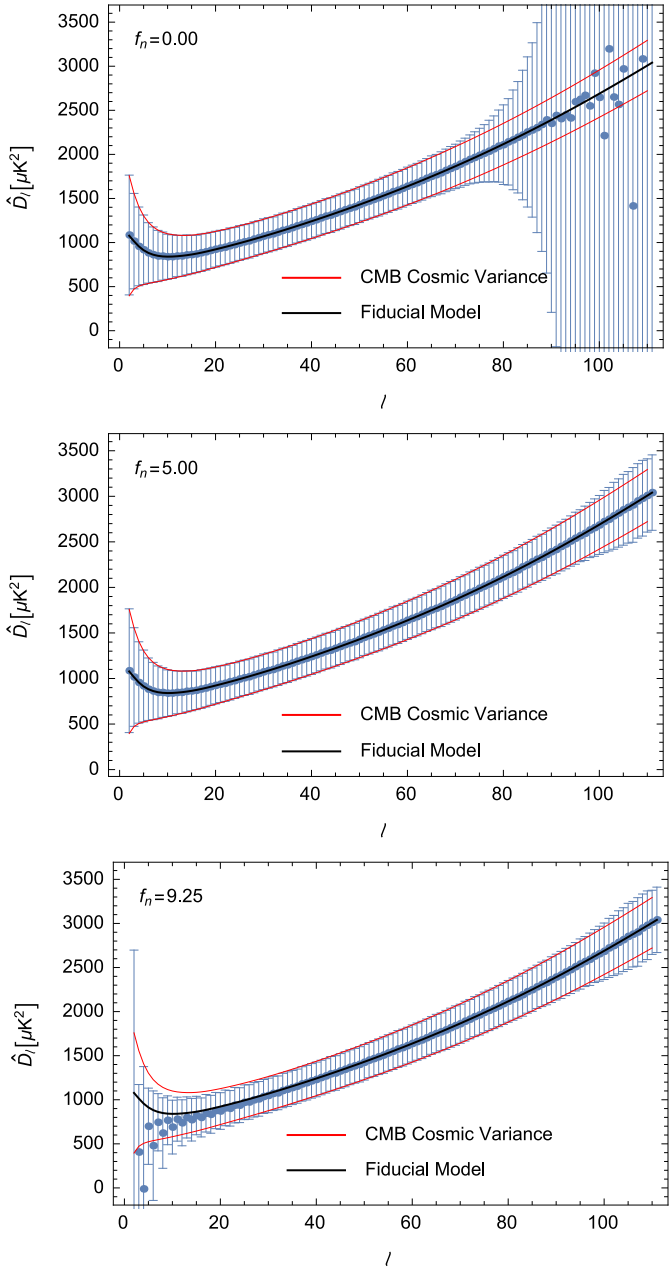

Figure 9. Power spectrum estimation given by the QML method for three different levels of noise, $f_n = \{0, 5, 9.25\}$.The average and 1σ error bars have been obtained from a set of 10.000 simulations.

error bar criterion gives the lowest value for the error size, the determinant departs from unity at the sixth decimal position (in the worst case), and the hypothesis test shows consistency with the expected theoretical distribution.

For a generic application, one could give some general considerations to proceed in order to have a regular covariance matrix and to help establishing the appropriate level of regularizing noise, if necessary, at each case:

1. Taking into account the number of pixels, the symmetries and if there is a mask, cal-

f_n	% noise	$\langle\sigma_\ell^{QML}/\sigma_\ell^{CV}\rangle_\ell$	p-value	$\lvert\mathbf{CC}^{-1}\rvert$	$-\log\left(\mathrm{abs}\left(1-\lvert\mathbf{CC}^{-1}\rvert\right)\right)$
0	2.08	2.54	0.63	1.00000000006	10.22
1	0.66	1.16	0.93	1.0000000007	9.13
2	0.21	1.02	0.66	1.000000003	8.49
3	6.6×10^{-2}	1.01	0.73	0.999999993	8.16
4	2.1×10^{-2}	1.01	0.73	1.000001	5.98
5	6.6×10^{-3}	1.01	0.73	0.999998	5.95
6	2.1×10^{-3}	1.01	0.73	1.000009	5.05
7	6.6×10^{-4}	1.01	0.60	1.0002	3.66
8	2.1×10^{-4}	1.01	0.11	0.97	1.50
9	6.6×10^{-5}	1.01	$\sim10^{-15}$	1.27×10^{36}	-36.10
9.25	4.9×10^{-5}	1.13	$\sim10^{-15}$	-1.12×10^{299}	-299.05
10	2.1×10^{-5}	$\sim7\times10^{5}$	$\sim10^{-14}$	∞	$-\infty$

Table 11. Summary of statistical tests obtained from 10.000 CMB simulations (at $N_{\rm side}=32$) with different levels of regularizing noise. The first column shows the value of the noise parameter f_n, $\sigma^2_{noise}=10^{-f_n}$. The second column gives the percentage of noise with respect to the dispersion of the CMB signal, i.e., $100\times\sigma_{noise}/\sqrt{S_{ii}}$. The third column shows the average over ℓ of the errors on the estimation of D_ℓ divided by those corresponding to the cosmic variance, eq. (8.4). The p-value corresponds to the probability that the quantity $\mathbf{x}^t\mathbf{C}^{-1}\mathbf{x}$ follows the expected χ^2 distribution according to the Cramér von Mises test. The two last columns show the results in relation to the determinant of $\lvert\mathbf{CC}^{-1}\rvert$.

culate the minimal theoretical multipole ℓ_{tm} up to which is necessary to sum in the calculus of $\mathbf{C}$ in order to get a regular matrix, using the adequate theoretical expression among the ones given in this paper.

2. If the real value up to which we sum in the calculation of $\mathbf{C}$, $\ell_{\rm max}$, is lower than the previously determined multipole, ℓ_{tm}, noise certainly needs to be added. Even if it is not lower, we might need to add some regularizing noise due to numerical errors.

3. If necessary, add an amount of noise. Table 11 may help to choose an initial guess.

4. Calculate $\mathbf{CC}^{-1}$ and evaluate how much it deviates from unity. One should bear in mind that a very good determinant can also be the consequence of adding an excessive amount of noise.

5. If the determinant is good, study the performance of the considered application (in our case the QML method) for this covariance matrix and compare it with the expected theoretical result.

6. If either the value of the determinant or the performance of your application is not as good as expected, iterate by changing the amount of regularizing noise until both goals are achieved.

9 Conclusions

We have presented a comprehensive study of the regularity of the covariance matrix $\mathbf{C}$ of a discretized field on the sphere. For a general case, we have shown that a necessary condition for the determinant of $\mathbf{C}$ to be different from zero is that the number of considered harmonics

is equal or greater than the number of pixels. The presence of specific symmetries for the considered pixelization or the use of a mask that excludes some regions of the sphere also impose additional constraints on the rank of $\mathbf{C}$. Along this work, five different expressions that establish limits on the maximum rank achieved by the covariance matrix are presented; they depend on the number of pixels, the number of spherical harmonics, the kind of symmetries of the considered pixelization and the presence of a mask.

When putting in practice these expressions for five different pixelizations proposed within the context of CMB analysis (`Cube`, `Icosahedron`, `Igloo`, `GLESP` and `HEALPix`), we have found that the particular properties of the location of the pixels can lead to a reduction of the rank of the covariance matrix with respect to the maximum rank allowed by the previously derived constraints. Interestingly, among the five studied pixelizations, `HEALPix` seems to present a lower reduction of the rank than the rest of pixelizations, which should help to achieve the regularity of the covariance matrix more easily.

We have also tested that numerical error propagation can give rise to a loss of rank, which would produce a singular covariance matrix in cases where this is not expected theoretically. By studying this effect with different numerical precisions, it is possible to differentiate whether the reduction of the rank is due to the propagation of numerical errors or to an intrinsically singular covariance matrix. As it is well known, a possible solution to mitigate the effect of numerical errors is to add some level of uncorrelated noise in order to regularize the covariance matrix. We have tested that even small levels of noise can be sufficient, although the particular value of the required noise will depend on the considered case.

We have also considered a practical case in which the calculation of the inverse of $\mathbf{C}$ is required, namely, the estimation of the CMB temperature power spectrum using the QML estimator. In particular, we have considered simulations containing CMB and different levels of noise using the `HEALPix` pixelization at resolution $N_{\rm side} = 32$. The optimal level of noise which needs to be included to obtain a regular matrix without degrading the quality of the data has been investigated in detail. We have studied particularly the behaviour of three different statistics in order to evaluate the quality of the results versus different levels of regularizing noise: the value of the determinant of $\mathbf{C}\mathbf{C}^{-1}$, a hypothesis test to study the distribution of the quantity $\eta = \mathbf{x}^t\mathbf{C}^{-1}\mathbf{x}$ (which should follow a χ^2 distribution if $\mathbf{x}$ represents Gaussian random fields) and the increment in the error of the estimation of the power spectrum with respect to the ideal case (given by the cosmic variance). The first conclusion from this particular exercise is that some level of noise, even if small, must be introduced in order to get a regular matrix, since numerical errors make the matrix singular even if this was not expected from the theoretical point of view. As the level of noise increases, the determinant and the hypothesis test indicate that the covariance matrix becomes more regular (for instance, it is observed that the determinant of $\mathbf{C}\mathbf{C}^{-1}$ departs less from unity). However, increasing the level of noise also degrades the quality of the data, which is reflected in the increment of the error in the estimation of the CMB power spectrum with the QML estimator. Also note that the error of this estimator can give good results even if the determinant criterion is bad. Therefore, for the sake of consistency, it becomes necessary to look simultaneously at all the statistics in order to establish the optimal level of noise for the error in the QML estimation to be as small as possible, while ensuring the covariance matrix is well behaved. For this particular case, this can be achieved with a level of noise as small as ~ 0.01 per cent with respect to the CMB dispersion (see table 11), although the particular value will depend on the considered case as well as on the required precision for the covariance matrix.

Finally, some general guidelines concerning the steps to follow to get a regular matrix

for a generic application are given in section 8.

A Study of the determinant of C

According to eq. (2.10), we can expand the determinant of **C** as a sum of determinants of matrices whose columns are the spherical harmonics calculated at the different pixels of the image. If one determinant in the sum is not null, there will be other $n! - 1$ terms that are not zero, corresponding to the permutations of its columns. However, in principle, it could happen that the sum of all these elements is zero. In this appendix we will calculate this sum and show that the result is a real, positive number.

Let us suppose that we have a particular collection of values $\{\mu_1, \mu_2, \ldots, \mu_n\}$ such that the corresponding determinant in eq. (2.10) is not null; of course, the indices must be different and correspond to a collection of linearly independent spherical harmonics. For the sake of simplicity, let us reassign labels to the spherical harmonics in such a way that now Y_{μ_i} is labelled as Y_i, so we have a matrix whose n columns are the n spherical harmonics $Y_i, i = 1, \ldots n$ evaluated in the n pixels of the map. Let us define D and **M**:

$$D \equiv \det(\mathbf{M}) \equiv \det \begin{pmatrix} Y_{11} & Y_{21} & \cdots & Y_{n1} \\ Y_{12} & Y_{22} & \cdots & Y_{n2} \\ \vdots & \vdots & & \vdots \\ Y_{1n} & Y_{2n} & \cdots & Y_{nn} \end{pmatrix}. \tag{A.1}$$

In the concatenated summations in eq. (2.10) there are another $n! - 1$ no null terms given by permutations of the columns of the matrix in eq. (A.1), whose determinants take values $\pm D$ depending on the signature of the permutation. Let S be the contribution to the determinant of **C** of the terms coming from those permutations, let P_n be the collection of permutations of n elements, and let us also relabel C_{μ_i} in eq. (2.10) as C_i. The summation extends over the permutations P_n, and:

$$\begin{aligned} S &= \sum_{\sigma \in P_n} \left[\prod_{i=1}^{n} C_i\right] \left[\prod_{i=1}^{n} Y^*_{\sigma_i i}\right] \operatorname{sign}(\sigma)\, D \\ &= D \left[\prod_{i=1}^{n} C_i\right] \det(\mathbf{M}^*) \\ &= \left[\prod_{i=1}^{n} C_i\right] |D|^2. \end{aligned} \tag{A.2}$$

Note that in order to get to the second line of the equation, we have taken out of the sum the constant D as well as the factors coming from the power spectrum that multiplies each permutation in eq. (2.10), since these factors only depend on the spherical harmonics in the permutation and not on its order. In this way we have identified the remaining sum as Leibniz's formula for the determinant of $\mathbf{M}^*$. Taking into account that determinant and conjugate commute, we get to the final expression of the previous equation.

Therefore, assuming that there are enough non-zero C_ℓ's, if we are able to find a collection of spherical harmonics such that $D \neq 0$, we have:

$$\det(\mathbf{C}) > 0. \tag{A.3}$$

Finally, let us calculate the full value of the determinant of $\mathbf{C}$. If we consider n points on the sphere and N spherical harmonics, we can find as many different sets of n spherical harmonics as the number of n-combinations of an N-set. Since the expression (A.2) gives the generic contribution to the determinant of $\mathbf{C}$ of a set of n harmonics, if we call σ to one of the combinations, and S_σ to the sum in eq. (A.2) for this combination, then:

$$\det(\mathbf{C}) = \sum_\sigma S_\sigma = \sum_\sigma \left(\prod_{i=1}^{n} C_{\sigma_i} \right) |D_\sigma|^2. \tag{A.4}$$

B S_I symmetry: $\mathbf{r} \to -\mathbf{r}$

The spherical harmonics satisfy

$$Y_{\ell m}(-z, \phi + \pi) = (-1)^\ell Y_{\ell m}(z, \phi). \tag{B.1}$$

If for each pixel with coordinates (z, ϕ) there exists a pixel with coordinates $(-z, \phi + \pi)$, the matrix in eq. (3.1) simplifies notably. This can be easily seen considering the simple case with $\ell = 1$ and four pixels:

$$\mathbf{Y} = \begin{pmatrix} Y_1^{-1}(\mathbf{r}_1) & Y_1^0(\mathbf{r}_1) & Y_1^1(\mathbf{r}_1) \\ Y_1^{-1}(\mathbf{r}_2) & Y_1^0(\mathbf{r}_2) & Y_1^1(\mathbf{r}_2) \\ Y_1^{-1}(\mathbf{r}_3) & Y_1^0(\mathbf{r}_3) & Y_1^1(\mathbf{r}_3) \\ Y_1^{-1}(\mathbf{r}_4) & Y_1^0(\mathbf{r}_4) & Y_1^1(\mathbf{r}_4) \end{pmatrix}. \tag{B.2}$$

If the pixels are opposed pairwise, $\mathbf{r}_3 = -\mathbf{r}_1$ y $\mathbf{r}_4 = -\mathbf{r}_2$, then the matrix of eq. (B.2) is a rank 2 matrix, since we have only two linearly independent rows:

$$\mathbf{Y} = \begin{pmatrix} Y_1^{-1}(\mathbf{r}_1) & Y_1^0(\mathbf{r}_1) & Y_1^1(\mathbf{r}_1) \\ Y_1^{-1}(\mathbf{r}_2) & Y_1^0(\mathbf{r}_2) & Y_1^1(\mathbf{r}_2) \\ -Y_1^{-1}(\mathbf{r}_1) & -Y_1^0(\mathbf{r}_1) & -Y_1^1(\mathbf{r}_1) \\ -Y_1^{-1}(\mathbf{r}_2) & -Y_1^0(\mathbf{r}_2) & -Y_1^1(\mathbf{r}_2) \end{pmatrix}. \tag{B.3}$$

With the help of this property we can notably simplify the matrix $\mathbf{Y}$. But let us first define an operator that will simplify the notation in the coming expression. Suppose that we have selected a certain pixel collection, indexed from 1 to k, and a set of harmonics, represented by Y_{LM}, that contains U elements indexed from 1 to U. The operator $\otimes$ constructs the block obtained by applying all the harmonics of the set on the selected pixels:

$$Y_{LM} \otimes \begin{pmatrix} \mathbf{r}_1 \\ \vdots \\ \mathbf{r}_k \end{pmatrix}_{k \times U} \equiv \begin{pmatrix} Y_{\ell_1 m_1}(\mathbf{r}_1) & \cdots & Y_{\ell_U m_U}(\mathbf{r}_1) \\ \vdots & & \vdots \\ Y_{\ell_1 m_1}(\mathbf{r}_k) & \cdots & Y_{\ell_U m_U}(\mathbf{r}_k) \end{pmatrix}. \tag{B.4}$$

Going back to $\mathbf{Y}$ and considering the case of n pixels in the pixelization that fully accomplish the S_I symmetry, $\mathbf{r}_{i+n/2} = -\mathbf{r}_i$, $i = 1 \ldots n/2$, if we reorder the spherical harmonics in such a way that the ones with even ℓ occupy the first columns and those with odd ℓ occupy the last

columns, $\mathbf{Y}$ becomes:

$$\mathbf{Y} = \begin{pmatrix} Y_{\ell_e} \otimes \begin{pmatrix} \mathbf{r}_1 \\ \vdots \\ \mathbf{r}_{n/2} \end{pmatrix}_{n/2\times N_e} & Y_{\ell_o} \otimes \begin{pmatrix} \mathbf{r}_1 \\ \vdots \\ \mathbf{r}_{n/2} \end{pmatrix}_{n/2\times N_o} \\ Y_{\ell_e} \otimes \begin{pmatrix} \mathbf{r}_{n/2+1} \\ \vdots \\ \mathbf{r}_{n} \end{pmatrix}_{n/2\times N_e} & Y_{\ell_o} \otimes \begin{pmatrix} \mathbf{r}_{n/2+1} \\ \vdots \\ \mathbf{r}_{n} \end{pmatrix}_{n/2\times N_o} \end{pmatrix}, \tag{B.5}$$

where ℓ_e and ℓ_o represent the set of spherical harmonics with even and odd ℓ respectively. The corresponding numbers of harmonics in each block are given by N_e and N_o (see eq. (3.5)).

Taking into account the symmetry of pixels and spherical harmonics, we have:

$$\mathbf{Y} = \begin{pmatrix} Y_{\ell_e} \otimes \begin{pmatrix} \mathbf{r}_1 \\ \vdots \\ \mathbf{r}_{n/2} \end{pmatrix}_{n/2\times N_e} & Y_{\ell_o} \otimes \begin{pmatrix} \mathbf{r}_1 \\ \vdots \\ \mathbf{r}_{n/2} \end{pmatrix}_{n/2\times N_o} \\ Y_{\ell_e} \otimes \begin{pmatrix} \mathbf{r}_1 \\ \vdots \\ \mathbf{r}_{n/2} \end{pmatrix}_{n/2\times N_e} & -Y_{\ell_o} \otimes \begin{pmatrix} \mathbf{r}_1 \\ \vdots \\ \mathbf{r}_{n/2} \end{pmatrix}_{n/2\times N_o} \end{pmatrix}. \tag{B.6}$$

It is possible to substitute the first $n/2$ rows r_i by the linear combination $\frac{1}{2}(r_i + r_{i+n/2})$, $i = 1, \ldots, n/2$. Similarly, the second half of rows can be replaced by $\frac{1}{2}(r_{i-n/2} - r_i)$, $i = n/2+1, \ldots, n$. With this transformation, one finds:

$$\mathbf{Y} \to \begin{pmatrix} Y_{\ell_e} \otimes \begin{pmatrix} \mathbf{r}_1 \\ \vdots \\ \mathbf{r}_{n/2} \end{pmatrix}_{n/2\times N_e} & \mathbf{0}_{n/2\times N_o} \\ \mathbf{0}_{n/2\times N_e} & Y_{\ell_o} \otimes \begin{pmatrix} \mathbf{r}_1 \\ \vdots \\ \mathbf{r}_{n/2} \end{pmatrix}_{n/2\times N_o} \end{pmatrix}. \tag{B.7}$$

Therefore, the rank of the matrix is equal to the sum of the ranks of the two diagonal blocks above. Each of these ranks is less or equal than the minimum between the number of rows ($\leq n/2$) and the number of columns (N_e or N_o), i.e.,

$$\mathrm{rank}(\mathbf{Y}) \leq \min\left(N_e, n/2\right) + \min\left(N_o, n/2\right), \tag{B.8}$$

which corresponds to the constraint R_1 presented in section 3.1.

C S_{II} symmetry: $\phi \to \phi + \pi$

Another interesting property of the spherical harmonics is:

$$Y_{\ell m}(z, \phi + \pi) = (-1)^m Y_{\ell m}(z, \phi). \tag{C.1}$$

Let us assume that we have a pixelization that satisfy the previous symmetry S_I. If for each point in the pixelization with coordinates (z, ϕ) there is another point with coordinates $(z, \phi + \pi)$, then it is possible to further simplify the matrix of eq. (B.7). In order to do this, one should first note that the non-zero blocks are evaluated only on the first half of the pixels. All pixels with $z \neq 0$ that are included in these blocks have their symmetric pair $\phi \to \phi + \pi$ also in the first half of pixels, which allows one to use symmetry S_{II} to reduce the size of the non-zero blocks. However, the case with $z = 0$ needs to be addressed separately. For these points, the corresponding $\phi \to \phi + \pi$ pixel satisfies also $\mathbf{r} \to -\mathbf{r}$, and therefore it has been removed out of the matrix during the transformations that led to the matrix of eq. (B.7). Therefore, for those positions with $z = 0$, the pixel symmetric with respect to the S_{II} symmetry is not present in the non-zero blocks and can not be used to further simplify the matrix of eq. (B.7).

Fortunately, there is another interesting property of the spherical harmonics that can be used in this case. If ℓ is even and m is odd, or if ℓ is odd and m is even, then $Y_{\ell m}(z = 0, \phi) = 0$. Let us assume that when applying the symmetry S_I, we have kept the first $n/2$ pixels (those with $z > 0$, and those with $z = 0$ and $0 \leq \phi < \pi$). Let us now reorder the spherical harmonics (i.e., the columns of matrix $\mathbf{Y}$) in a sequence such that the values (ℓ, m) are arranged in the following combinations: (even, odd), (even, even), (odd, odd), and finally (odd, even). After this rearrangement, the even ℓ block of matrix of eq. (B.7) becomes:

$$\mathbf{Y}_e = \begin{pmatrix} Y_{\ell_e m_o} \otimes \begin{pmatrix} \mathbf{r}_1 \\ \vdots \\ \mathbf{r}_k \end{pmatrix}_{k \times N_{eo}} & Y_{\ell_e m_e} \otimes \begin{pmatrix} \mathbf{r}_1 \\ \vdots \\ \mathbf{r}_k \end{pmatrix}_{k \times N_{ee}} \\ \\ \mathbf{0}_{u \times N_{eo}} & Y_{\ell_e m_e} \otimes \begin{pmatrix} \mathbf{r}_{k+1} \\ \vdots \\ \mathbf{r}_{k+u} \end{pmatrix}_{u \times N_{ee}} \end{pmatrix}, \tag{C.2}$$

where we have also separated the rows corresponding to k pixels with $z > 0$ from the u positions with $z = 0$, thus $k + u = n/2$.

N_{eo} is the number of spherical harmonics with even ℓ and odd m, and N_{ee} is the number of spherical harmonics with even ℓ and even m. Using eq. (C.1) and dividing the k pixels with $z > 0$ in two halves, one with $0 \leq \phi < \pi$ and another one with $\pi \leq \phi < 2\pi$, the block of eq. (C.2) can be transformed:

$$\mathbf{Y}_e \to \begin{pmatrix} Y_{\ell_e m_o} \otimes \begin{pmatrix} \mathbf{r}_1 \\ \vdots \\ \mathbf{r}_{k/2} \end{pmatrix}_{k/2 \times N_{eo}} & \mathbf{0}_{k/2 \times N_{ee}} \\ \\ \mathbf{0}_{k/2 \times N_{eo}} & Y_{\ell_e m_e} \otimes \begin{pmatrix} \mathbf{r}_1 \\ \vdots \\ \mathbf{r}_{k/2} \end{pmatrix}_{k/2 \times N_{ee}} \\ \\ \mathbf{0}_{u \times N_{eo}} & Y_{\ell_e m_e} \otimes \begin{pmatrix} \mathbf{r}_{k+1} \\ \vdots \\ \mathbf{r}_{k+u} \end{pmatrix}_{u \times N_{ee}} \end{pmatrix}, \tag{C.3}$$

where we have operated in an analogous way to that used in the transformation that led to the matrix of eq. (B.7). The odd ℓ block of this matrix can also be simplified in the same manner, until $\mathbf{Y}$ is finally reduced to a four diagonal block matrix. The total rank is the sum of the ranks of the four blocks:

$$\begin{aligned}\mathrm{rank}(\mathbf{Y}) \leq & \min(N_{eo}, k/2) + \min(N_{ee}, k/2+u) \\ & + \min(N_{oo}, k/2+u) + \min(N_{oe}, k/2),\end{aligned} \tag{C.4}$$

where N_{oo} y N_{oe} are the number of spherical harmonics with odd ℓ and m and with odd ℓ and even m, respectively.

D S_{III} symmetry: $\phi \to \phi + \pi/2$

A third interesting symmetry relation of the spherical harmonics is:

$$Y_{\ell m}(\theta, \phi + \pi/2) = i^m Y_{\ell m}(\theta, \phi)\,. \tag{D.1}$$

Again, let us assume that we have a pixelization that satisfy the symmetries S_I and S_{II} and, therefore, we can transform the matrix $\mathbf{Y}$ into a matrix with four diagonal blocks as the one described in eq. (C.3). If, in addition, for each point in the pixelization with coordinates (z, ϕ) there is another point with coordinates $(z, \phi+\pi/2)$, it is then possible to subdivide each block into two diagonal sub-blocks. To do that, we need to rearrange the pixels and spherical harmonics properly, and take linear combinations similar to the ones described in appendix C. We show as an example the transformation of the block of the spherical harmonics of even ℓ and odd m of eq. (C.3):

$$\mathbf{Y}_{eo} = Y_{\ell_e m_o} \otimes \begin{pmatrix} \mathbf{r}_1 \\ \vdots \\ \mathbf{r}_{k/2} \end{pmatrix}_{k/2 \times N_{eo}}\,, \tag{D.2}$$

into:

$$\mathbf{Y}_{eo} \to \begin{pmatrix} Y_{\ell_e m_1} \otimes \begin{pmatrix} \mathbf{r}_1 \\ \vdots \\ \mathbf{r}_{k/4} \end{pmatrix}_{k/4 \times N_{e1}} & \mathbf{0}_{k/4 \times N_{e3}} \\ \mathbf{0}_{k/4 \times N_{e1}} & Y_{\ell_e m_3} \otimes \begin{pmatrix} \mathbf{r}_1 \\ \vdots \\ \mathbf{r}_{k/4} \end{pmatrix}_{k/4 \times N_{e3}} \end{pmatrix}. \tag{D.3}$$

N_{e1} and N_{e3} are the number of spherical harmonics with $i^m = i$ and $i^m = -i$, respectively, and m_1 and m_3 indicate the corresponding sets of indices. Note that, in this case, to obtain zero blocks the imaginary unit i has to be introduced in the linear combinations of rows. The block corresponding to the spherical harmonics with even ℓ and m in eq. (C.3), and those with odd ℓ can be similarly transformed. Finally, the matrix is divided into eight diagonal blocks whose total rank is constrained by eq. (3.12).

E Rank expression under the presence of a mask

In order to prove the constraint given by eq. (7.4), we start from the full matrix $\mathbf{Y}$:

$$\mathbf{Y} = \begin{pmatrix} Y_{1,1} & \cdots & Y_{N,1} \\ \vdots & & \vdots \\ Y_{1,n} & \cdots & Y_{N,n} \end{pmatrix}. \tag{E.1}$$

Let us consider that we have n valid pixels allowed by the mask that correspond to n_p paired pixels (i.e. that fulfil the S_I symmetry) and n_u unpaired pixels, $n = n_p + n_u$. Let us also assume that there are N_e and N_o spherical harmonics of even and odd ℓ respectively. By properly ordering the spherical harmonics and the pixels, and after taking linear combinations of the n_p rows as we did in appendix B, the matrix of eq. (E.1) can be converted into:

$$\mathbf{Y} \to \begin{pmatrix} \mathbf{Y}^{even}_{n_p/2\times N_e} & \mathbf{0}_{n_p/2\times N_o} \\ \mathbf{0}_{n_p/2\times N_e} & \mathbf{Y}^{odd}_{n_p/2\times N_o} \\ \mathbf{Y}^{even}_{n_u\times N_e} & \mathbf{Y}^{odd}_{n_u\times N_o} \end{pmatrix} \equiv \begin{pmatrix} \mathbf{Y}^e_p & \mathbf{0} \\ \mathbf{0} & \mathbf{Y}^o_p \\ \mathbf{Y}^e_u & \mathbf{Y}^o_u \end{pmatrix}. \tag{E.2}$$

If the rank of the block $\mathbf{Y}^e_p$ is R_e and the one of $\mathbf{Y}^o_p$ is R_o, we have:

$$R_e \leq \min(n_p/2, N_e), \qquad R_o \leq \min(n_p/2, N_o), \tag{E.3}$$

since the rank of each block has to be less or equal than the minimum between the number of rows and the number of columns.

Taking linear combinations, the blocks $\mathbf{Y}^e_p$ and $\mathbf{Y}^o_p$ of the previous matrix can be transformed into diagonal blocks with as many no null elements as their respective ranks, R_e and R_o. Showing it explicitly for $\mathbf{Y}^e_p$, and substituting $\mathbf{Y}^o_p$ by its diagonal form $\mathbf{D}^o_p$, we have:

$$\mathbf{Y} \to \begin{pmatrix} d^e_{11} & 0 & \cdots & 0 & & \\ 0 & d^e_{22} & \cdots & 0 & \mathbf{0} & \\ \vdots & \vdots & \ddots & \vdots & & \mathbf{0} \\ 0 & 0 & \cdots & d^e_{R_eR_e} & & \\ & & \mathbf{0} & & \mathbf{0} & \\ & & \mathbf{0} & & \begin{matrix} \mathbf{D}^o_p & \mathbf{0} \\ \mathbf{0} & \mathbf{0} \end{matrix} & \\ & & \mathbf{Y}^e_u & & \mathbf{Y}^o_u & \end{pmatrix}. \tag{E.4}$$

Note that some of the zero blocks around $\mathbf{D}^e_p$ and $\mathbf{D}^o_p$ will not appear if the equality is fulfilled in eq. (E.3).

Furthermore, using the diagonal blocks, we can obtain R_e zeros in the $\mathbf{Y}_u^e$ block and R_o zeros in the $\mathbf{Y}_u^o$ block. Therefore, the matrix can be further simplified:

$$\mathbf{Y} \to \begin{pmatrix} \mathbf{D}_p^e & \mathbf{0} & & \\ \mathbf{0} & \mathbf{0} & \mathbf{0} & \\ & & \mathbf{D}_p^o & \mathbf{0} \\ \mathbf{0} & & \mathbf{0} & \mathbf{0} \\ \mathbf{0} & \mathbf{Y'}_u^e & \mathbf{0} & \mathbf{Y'}_u^o \end{pmatrix}, \tag{E.5}$$

where the $\mathbf{Y'}_u^e$ and $\mathbf{Y'}_u^o$ blocks have $N_e - R_e$ columns and $N_o - R_o$ columns, respectively. Finally, reordering the rows and columns, we obtain:

$$\mathbf{Y} \to \begin{pmatrix} \mathbf{D}_p^e & \mathbf{0} & \mathbf{0} & \mathbf{0} \\ \mathbf{0} & \mathbf{D}_p^o & \mathbf{0} & \mathbf{0} \\ \mathbf{0} & \mathbf{0} & \mathbf{Y'}_u^e & \mathbf{Y'}_u^o \\ \mathbf{0} & \mathbf{0} & \mathbf{0} & \mathbf{0} \end{pmatrix}. \tag{E.6}$$

Inspecting this matrix, we can easily derive the constraint given in eq. (7.2). For the rank($\mathbf{C}$) to be maximum, i.e. rank($\mathbf{C}$) = rank($\mathbf{Y}$) = n, $\mathbf{Y}$ needs to have n independent rows. Therefore, in this case, we would get a matrix like the one of eq. (E.6) but without the last row of zero blocks. Moreover, given that the block $\mathbf{D}_p^e$ has $n_p/2$ rows, it must also have at least $n_p/2$ linear independent columns in order to achieve the maximum rank. Since all of its columns are constructed in terms of spherical harmonics of even ℓ, then $N_e \geq n_p/2$ must be satisfied. Similarly, the same reasoning applies to block $\mathbf{D}_p^o$, finding $N_o \geq n_p/2$.

Let us now study the rank of the matrix in eq. (E.6) for any $\ell_{\max}$. Its rank is the sum of the ranks of the blocks $\mathbf{D}_p^e$, $\mathbf{D}_p^o$ and ($\mathbf{Y'}_u^e\, \mathbf{Y'}_u^o$). Taking into account eq. (E.3) and since the block ($\mathbf{Y'}_u^e\, \mathbf{Y'}_u^o$) has n_u rows and $L^* = N_e - R_e + N_o - R_o$ columns, we get the limit:

$$\begin{aligned} \text{rank}(\mathbf{Y}) &\leq R_e + R_o + \min(n_u, L^*) \\ &\leq \min(n_p/2, N_e) + \min(n_p/2, N_o) + \min(n_u, L^*). \end{aligned} \tag{E.7}$$

However this expression depends through L^* on the ranks R_e and R_o which are, in principle, unknown. It would be more convenient to have a more general constraint which did not depend on these ranks. With this aim, let us consider a new parameter, L, defined as:

$$L = N_e - \min(n_p/2, N_e) + N_o - \min(n_p/2, N_o). \tag{E.8}$$

Taking into account eq. (E.3), it becomes apparent that $L^* \geq L$ and $\min(n_u, L^*) \geq \min(n_u, L)$. Therefore, it is not obvious whether the expression (E.7) is still valid when replacing L^* by L (except in the trivial case $L^* = L$).

Let us study in more detail the case $L^* > L$. We suppose $L^* = L + t$, with $t \geq 1$. In this case, R_e or R_o (or both) are lower than their possible maximum value given by the geometrical dimensions of the corresponding blocks. For the sake of simplicity, and without loss of generality, let us assume that $R_e = \min(n_p/2, N_e) - t$ (note that if both R_e and R_o are lower than their maximum geometrical value, the same reasoning would be done twice, with t_e and t_o, $t = t_e + t_o$). In this situation, we have:

$$\begin{aligned} \text{rank}(\mathbf{Y}) &\leq R_e + R_o + \min(n_u, L^*) \\ &\leq \min(n_p/2, N_e) - t + \min(n_p/2, N_o) \\ &\quad + \min(n_u, L^*). \end{aligned} \tag{E.9}$$

Let us now focus on the value of the last term, $\min(n_u, L^*)$, and consider the two possible complementary cases $n_u \geq L^*$ and $n_u < L^*$.

1. If $n_u \geq L^*$, then $\min(n_u, L^*) = L^* = L + t$, and $\min(n_u, L) = L$. Expression (E.9) becomes:

$$\begin{aligned} \text{rank}(\mathbf{Y}) &\leq \min(n_p/2, N_e) - t + \min(n_p/2, N_o) + L + t \\ &= \min(n_p/2, N_e) + \min(n_p/2, N_o) + \min(n_u, L). \end{aligned} \tag{E.10}$$

2. Conversely, if $n_u < L^*$, expression (E.9) becomes:

$$\text{rank}(\mathbf{Y}) \leq \min(n_p/2, N_e) + \min(n_p/2, N_o) + n_u - t. \tag{E.11}$$

   Since $L < L^*$, if $n_u < L^*$ we have again two complementary possibilities: $n_u \leq L$ and $n_u > L$.

   (a) Let us first suppose that $n_u \leq L$, which implies $\min(n_u, L) = n_u$. In this case, from eq. (E.11) we have:

$$\begin{aligned} \text{rank}(\mathbf{Y}) &< \min(n_p/2, N_e) + \min(n_p/2, N_o) + n_u \\ &= \min(n_p/2, N_e) + \min(n_p/2, N_o) + \min(n_u, L). \end{aligned} \tag{E.12}$$

   (b) Finally let us consider the case $n_u < L^*$ and $n_u > L$. As $L < n_u < L^* = L + t$, then $L - t < n_u - t < L$ and $\min(n_u, L) = L$. Therefore we can replace $n_u - t$ by L in expression (E.11) if we substitute the sign $\leq$ by $<$:

$$\begin{aligned} \text{rank}(\mathbf{Y}) &< \min(n_p/2, N_e) + \min(n_p/2, N_o) + L \\ &= \min(n_p/2, N_e) + \min(n_p/2, N_o) + \min(n_u, L). \end{aligned} \tag{E.13}$$

Since we have covered all the possible cases, this shows that we can write an upper limit on the rank of the masked case which does not depend on R_e and R_0 as:

$$\text{rank}(\mathbf{Y}) \leq \min(n_p/2, N_e) + \min(n_p/2, N_o) + \min(n_u, L). \tag{E.14}$$

which proves the validity of the constraint (7.4) given in section 7.

Acknowledgments

We acknowledge partial financial support from the Spanish *Ministerio de Economía y Competitividad* Projects Consolider-Ingenio 2010 CSD2010-00064, ESP2015-70646-C2-1-R and AYA2015-64508-P (MINECO/FEDER,UE). This research was also supported by the RADIOFOREGROUNDS project, funded by the European Comission's H2020 Research Infrastructures under the Grant Agreement 687312. We also thank CSIC for a Proyecto Intramural Especial (201550I027). The `HEALPix` package [19] was used throughout the data analysis.

References

[1] A. Klinger, *Approximate pseudoinverse solutions to ill-conditioned linear systems*, *Journal of Optimization Theory and Applications* **2** (1968), no. 2 117–124.

[2] M. Tegmark, *How to measure CMB power spectra without losing information*, *PhRvD* **55** (May, 1997) 5895–5907, [astro-ph/9611174].

[3] M. Zaldarriaga. Cosmic Microwave Background Polarization Experiments. *ApJ*, 503:1–15, August 1998, [astro-ph/9709271].

[4] **Planck** Collaboration, P. A. R. Ade, N. Aghanim, C. Armitage-Caplan, M. Arnaud, M. Ashdown, F. Atrio-Barandela, J. Aumont, C. Baccigalupi, A. J. Banday, and et al., *Planck 2013 results. XV. CMB power spectra and likelihood*, *A&A* **571** (Nov., 2014) A15, [arXiv:1303.5075].

[5] **Planck** Collaboration, N. Aghanim, M. Arnaud, M. Ashdown, J. Aumont, C. Baccigalupi, A. J. Banday, R. B. Barreiro, J. G. Bartlett, N. Bartolo, and et al., *Planck 2015 results. XI. CMB power spectra, likelihoods, and robustness of parameters*, *A&A* **594** (Sept., 2016) A11, [arXiv:1507.0270].

[6] G. Aslanyan, A. V. Manohar, and A. P. S. Yadav, *The topology and size of the universe from CMB temperature and polarization data*, *JCAP* **8** (Aug., 2013) 009, [arXiv:1304.1811].

[7] M. Tegmark, *Removing Real-World Foregrounds from Cosmic Microwave Background Maps*, *ApJ* **502** (July, 1998) 1–6, [astro-ph/9712038].

[8] H. K. Eriksen, A. J. Banday, K. M. Górski, and P. B. Lilje, *On Foreground Removal from the Wilkinson Microwave Anisotropy Probe Data by an Internal Linear Combination Method: Limitations and Implications*, *ApJ* **612** (Sept., 2004) 633–646, [astro-ph/0403098].

[9] H. K. Eriksen, G. Huey, R. Saha, F. K. Hansen, J. Dick, A. J. Banday, K. M. Górski, P. Jain, J. B. Jewell, L. Knox, D. L. Larson, I. J. O'Dwyer, T. Souradeep, and B. D. Wandelt, *A Reanalysis of the 3 Year Wilkinson Microwave Anisotropy Probe Temperature Power Spectrum and Likelihood*, *ApJ* **656** (Feb., 2007) 641–652, [astro-ph/0606088].

[10] **Planck** Collaboration, P. A. R. Ade, N. Aghanim, C. Armitage-Caplan, M. Arnaud, M. Ashdown, F. Atrio-Barandela, J. Aumont, C. Baccigalupi, A. J. Banday, and et al., *Planck 2013 results. XII. Diffuse component separation*, *A&A* **571** (Nov., 2014) A12, [arXiv:1303.5072].

[11] P. Vielva and J. L. Sanz, *Analysis of non-Gaussian cosmic microwave background maps based on the N-pdf. Application to Wilkinson Microwave Anisotropy Probe data*, *MNRAS* **397** (Aug., 2009) 837–848, [arXiv:0812.1756].

[12] A. Curto, E. Martínez-González, and R. B. Barreiro, *On the optimality of the spherical mexican hat wavelet estimator for the primordial non-gaussianity*, *MNRAS* **412** (2011), no. 2 1038–1046, [arXiv:1007.2181].

[13] M. Cruz, N. Turok, P. Vielva, E. Martínez-González, and M. Hobson, *A Cosmic Microwave Background Feature Consistent with a Cosmic Texture*, *Science* **318** (Dec., 2007) 1612–, [arXiv:0710.5737].

[14] **Planck** Collaboration, P. A. R. Ade, N. Aghanim, Y. Akrami, P. K. Aluri, M. Arnaud, M. Ashdown, J. Aumont, C. Baccigalupi, A. J. Banday, and et al., *Planck 2015 results. XVI. Isotropy and statistics of the CMB*, *A&A* **594** (Aug., 2016) A16, [arXiv:1506.0713].

[15] F. K. Chan and E. M. O'Neill, *Feasibility Study of a Quadrilateralized Spherical Cube Earth Data Base*, *Computer Sciences Corporation* (1975).

[16] M. Tegmark, *An Icosahedron-Based Method for Pixelizing the Celestial Sphere*, *ApJL* **470** (Oct., 1996) L81, [astro-ph/9610094].

[17] R. G. Crittenden, *Igloo Pixelizations of the Sky*, *Astrophysical Letters and Communications* **37** (2000) 377, [astro-ph/9811273].

[18] A. G. Doroshkevich, P. D. Naselsky, O. V. Verkhodanov, D. I. Novikov, V. I. Turchaninov, I. D. Novikov, P. R. Christensen, and L.-Y. Chiang, *Gauss-Legendre Sky Pixelization (glesp) for CMB Maps*, *International Journal of Modern Physics D* **14** (2005) 275–290, [astro-ph/0305537].

[19] K. M. Górski, E. Hivon, A. J. Banday, B. D. Wandelt, F. K. Hansen, M. Reinecke, and M. Bartelmann, *HEALPix: A Framework for High-Resolution Discretization and Fast Analysis of Data Distributed on the Sphere*, *ApJ* **622** (Apr., 2005) 759–771, [astro-ph/0409513].

[20] C. L. Bennett, A. J. Banday, K. M. Gorski, G. Hinshaw, P. Jackson, P. Keegstra, A. Kogut, G. F. Smoot, D. T. Wilkinson, and E. L. Wright, *Four-Year COBE DMR Cosmic Microwave Background Observations: Maps and Basic Results*, *ApJL* **464** (June, 1996) L1, [astro-ph/9601067].

[21] A. G. Doroshkevich, O. V. Verkhodanov, P. D. Naselsky, J. Kim, D. I. Novikov, V. I. Turchaninov, I. D. Novikov, L.-Y. Chiang, and M. Hansen, *The Gauss-Legendre Sky Pixelization for the CMB Polarization Glesp-Pol Errors due to Pixelization of the CMB Sky*, *International Journal of Modern Physics D* **20** (2011) 1053–1078, [arXiv:0904.2517].

[22] **Planck** Collaboration, P. A. R. Ade, N. Aghanim, M. Arnaud, M. Ashdown, J. Aumont, C. Baccigalupi, A. J. Banday, R. B. Barreiro, J. G. Bartlett, and et al., *Planck 2015 results. XIII. Cosmological parameters*, *A&A* **594** (Sept., 2016) A13, [arXiv:1502.0158].

[23] **BICEP2** Collaboration, Keck Array Collaboration, P. A. R. Ade, Z. Ahmed, R. W. Aikin, K. D. Alexander, D. Barkats, S. J. Benton, C. A. Bischoff, J. J. Bock, R. Bowens-Rubin, J. A. Brevik, I. Buder, E. Bullock, V. Buza, J. Connors, B. P. Crill, L. Duband, C. Dvorkin, J. P. Filippini, S. Fliescher, J. Grayson, M. Halpern, S. Harrison, S. R. Hildebrandt, G. C. Hilton, H. Hui, K. D. Irwin, J. Kang, K. S. Karkare, E. Karpel, J. P. Kaufman, B. G. Keating, S. Kefeli, S. A. Kernasovskiy, J. M. Kovac, C. L. Kuo, E. M. Leitch, M. Lueker, K. G. Megerian, T. Namikawa, C. B. Netterfield, H. T. Nguyen, R. O'Brient, R. W. Ogburn, IV, A. Orlando, C. Pryke, S. Richter, R. Schwarz, C. D. Sheehy, Z. K. Staniszewski, B. Steinbach, R. V. Sudiwala, G. P. Teply, K. L. Thompson, J. E. Tolan, C. Tucker, A. D. Turner, A. G. Vieregg, A. C. Weber, D. V. Wiebe, J. Willmert, C. L. Wong, W. L. K. Wu, and K. W. Yoon, *BICEP2/Keck Array. VII. Matrix Based E/B Separation Applied to Bicep2 and the Keck Array*, *ApJ* **825** (July, 2016) 66, [arXiv:1603.0597].

[24] J. R. Bond, A. H. Jaffe, and L. Knox, *Estimating the power spectrum of the cosmic microwave background*, *PhRvD* **57** (Feb., 1998) 2117–2137, [astro-ph/9708203].

[25] M. Tegmark and A. de Oliveira-Costa, *How to measure CMB polarization power spectra without losing information*, *PhRvD* **64** (Sept., 2001) 063001, [astro-ph/0012120].

[26] A. Gruppuso, A. de Rosa, P. Cabella, F. Paci, F. Finelli, P. Natoli, G. de Gasperis, and N. Mandolesi, *New estimates of the CMB angular power spectra from the WMAP 5 year low-resolution data*, *MNRAS* **400** (Nov., 2009) 463–469, [arXiv:0904.0789].

[27] F. Schiavon, F. Finelli, A. Gruppuso, A. Marcos-Caballero, P. Vielva, R. G. Crittenden, R. B. Barreiro, and E. Martínez-González, *An optimal estimator for the CMB-LSS angular power spectrum and its application to WMAP and NVSS data*, *MNRAS* **427** (Dec., 2012) 3044–3054, [arXiv:1203.3277].

[28] T. W. Anderson, *On the distribution of the two-sample cramer-von mises criterion*, *Ann. Math. Statist.* **33** (09, 1962) 1148–1159.